ACS PHYSICAL CHEMISTRY Au
AN OPEN ACCESS JOURNAL OF THE AMERICAN CHEMICAL SOCIETY

pubs.acs.org/physchemau
Perspective

Screening 2D Materials for Their Nanotoxicity toward Nucleic Acids and Proteins: An In Silico Outlook

Titas Kumar Mukhopadhyay, Anupam Ghosh, and Ayan Datta*

Cite This: ACS Phys. Chem Au 2024, 4, 97−121
Read Online

ABSTRACT: Since the discovery of graphene, two-dimensional (2D) materials have been anticipated to demonstrate enormous potential in bionanomedicine. Unfortunately, the majority of 2D materials induce nanotoxicity via disruption of the structure of biomolecules. Consequently, there has been an urge to synthesize and identify biocompatible 2D materials. Before the cytotoxicity of 2D nanomaterials is experimentally tested, computational studies can rapidly screen them. Additionally, computational analyses can provide invaluable insights into molecular-level interactions. Recently, various "*in silico*" techniques have identified these interactions and helped to develop a comprehensive understanding of nanotoxicity of 2D materials. In this article, we discuss the key recent advances in the application of computational methods for the screening of 2D materials for their nanotoxicity toward two important categories of abundant biomolecules, namely, nucleic acids and proteins. We believe the present article would help to develop newer computational protocols for the identification of novel biocompatible materials, thereby paving the way for next-generation biomedical and therapeutic applications based on 2D materials.

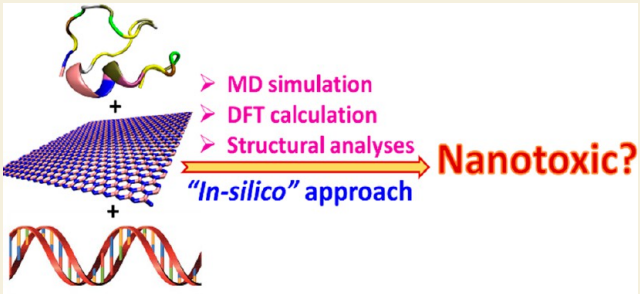

KEYWORDS: *Two-dimensional materials, nanotoxicity, biocompatibility, bionanomedicine, molecular dynamics simulations, computational chemistry*

1. INTRODUCTION

Ever since the discovery of Graphene, two-dimensional (2D) nanomaterials have revealed a cornucopia of novel material science and gained enormous research attention owing to their remarkable mechanical stability and unreactive nature along with fascinating optical, thermal, structural, and electronic properties.[1−6] High hopes have been placed on Graphene and analogous 2D materials for their outstanding applications in the realms of optoelectronics, sensing and separation technologies, electrochemistry, and energy storage.[6] Apart from the above-mentioned applications, 2D materials and their functionalized derivatives have been anticipated to have a plethora of applications in the domains of bionanomedicine, gene and drug delivery, tumor therapy, tissue engineering, sequencing of biomolecules, photothermal and photodynamic therapies, diagnostic imaging, theranostics, and surface enhanced Raman spectroscopy (SERS).[7−12] The emergence of 2D materials as an excellent choice for interaction with biomolecules ascended due to their flat surfaces, high surface-to-volume ratio, and tunable functionalities, despite the fact that hybrids of inorganic nanomaterials and biomolecules scarcely cohabitate in nature.[10]

One of the first demonstrations of the biomedical properties of 2D materials which intrigued material scientists and biologists alike was carried out by Dai et al. when they used graphene oxide (GO) as an efficient nanocarrier for cellular imaging and drug delivery.[13] GO has been conjugated with folic acid and SO_3H groups and then loaded with doxorubicin (DOX) and camptothecin (CPT), the hybrid system showing high cytotoxicity to human breast cancer cells.[14] Polyethylenimine (PEI) and chitosan-functionalized GO has been used as a gene delivery vector via condensation with plasmid DNA and siRNA.[15,16] Exploiting the fluorescent behavior of functionalized graphene, they have been widely employed as probes for diagnostic imaging.[17,18] Pushing forward the biomedical usage, graphene-based materials (GBMs) have been used as scaffolds for tissue engineering, cell culture, and bone regeneration therapy.[19,20] Nanopores in graphene and GO have been studied for their widespread applications in the sensing of biomolecules such as nucleotides, amino acids, antibodies, peptides, and adenosine triphosphate (ATP), among others.[21,22]

Received: September 12, 2023
Revised: November 4, 2023
Accepted: November 6, 2023
Published: November 22, 2023

Following the encouraging results of GBMs in biomedicine, researchers have turned their attention to other 2D materials, such as hexagonal boron nitride (*h*-BN), transition-metal dichalcogenides (TMDs), black phosphorene (BP), *h*2D-C_2N, and graphitic carbon nitride (g-C_3N_4), among others.[10,23−26] The first candidate, which has been expected to show a promising future in biomedicine, is *h*-BN. It is predicted that *h*-BN, having strong fluorescent behavior, may have potential usage in the realm of imaging technologies.[27] Alternatively, the flat unreactive surface of *h*-BN has been used for drug loading and delivery.[28] Similarly, BP has been explored for the controlled delivery of doxorubicin and platinum-based anticancer agents.[29] BP and its functionalized derivatives have been demonstrated for applications in surface-enhanced Raman scattering (SERS), photoacoustic and photothermal imaging, and combinatorial treatments.[29−31] TMDs have seen biomedical applications only recently, especially in the realm of biomolecular sequencing.[32] It has been reported that a nanopore in MoS_2 could perform "real-time" polynucleotide detection at a single nucleotide resolution, and MoS_2 nanoflakes have been used to develop glucose sensors.[33] On the other hand, WS_2 has been utilized to develop a testing kit to detect blood glucose level.[34] A novel TMD, TiS_2 has been predicted to have a prosperous future in theranostics, while TiO_2 nanoparticles have been used for nonevasive cancer treatment.[35,36] Another class of 2D materials which has recently witnessed biomedical research attention is the carbon-doped graphene-like 2D materials such as *h*2D-C_2N, graphitic carbon nitride (g-C_3N_4), C_3N, and C_5N, among others. Initial studies with these materials have suggested that they may display substantial potential in biomedical research; however, investigations related to these materials are still in infancy.[10,23,32,37]

Despite providing a bright glimmer of optimism in the field of bio-nanomedicine, many of these 2D materials have been proven to be nanotoxic, causing damage to biomolecules. A decade of in vitro and in vivo nanotoxicology research has demonstrated that nanomaterials often interact with biological systems in chemically and physically distinct ways.[8,10,23,38] Chemical reactions that occur during these interactions, such as oxidation, functional group interconversion, selenium/sulfur replacement, ligand modification, generation of reactive oxygen species (ROS), and ion-capture, among others, cause irreversible damage to the native structures that leads to serious biological anomalies. However, rather than chemical changes, the principal mode of interaction has been identified as noncovalent interactions.[38,39] Graphene and GO have been found to show antibacterial properties, destroying the bacterial cell membrane via lipid extraction.[40] GO has been found to exhibit size-dependent toxicity toward red blood cells and mammalian fibroblasts.[41] GBMs also rupture the secondary and tertiary structures of proteins and inhibit protein−protein interactions (PPIs).[41,42] Most of the toxic properties of graphene are also maintained in the case of *h*-BN. Cytotoxic effects of *h*-BN on lung alveoli cells and human embryonic kidney (HEK) cells have been found to be higher compared to carbon nanotubes.[43] *h*-BN nanosheets have been reported to reduce cell survival while also causing severe effects via intracellular ROS production and mitochondrial depolarization.[44,45] Similarly, polydispersed BP has been found to show selected antitumor and antimicrobial properties.[46,47] On the other hand, TMDs show lesser nanotoxic effects toward human epithelial carcinoma, pancreatic carcinoma, HeLa cells, lung carcinoma, and murine breast cancer cells compared to the above-mentioned materials.[48−50] BP was shown to have intermediate cytotoxicity between GO and TMDs against human lung cancer cells.[51]

It is evident from a thorough review of the literature that the majority of 2D materials exhibit cytotoxic behavior at the nanoscale, i.e., nanotoxicity. However, the extent of nanotoxicity inflicted by the 2D nanomaterials on biomolecules remains elusive since the number of experimental studies is significantly limited and they do not provide the molecular-level details of the underlying mechanism. As a result, the bionano research community is clamoring for a unified understanding of the mechanism that causes nanotoxicity. In addition, it is crucial to assess the biocompatibility of newer 2D materials as well as their impact on various categories of biomolecules including proteins, nucleic acids, biological receptors, and enzymes, among others. One of the alternatives to experimental verification of the cytotoxicity of 2D materials is *in silico* techniques, such as density functional theory (DFT) and molecular dynamics (MD) simulations. In recent years, these techniques, especially MD simulations, have been utilized to study the effects of 2D materials on biomolecules, leading to a comprehensive understanding of the induction of nanotoxicity. In this feature article, we describe the important computational protocols applied to infer the detrimental effects of 2D materials on two kinds of biomolecules, namely, nucleic acids and proteins. Any living organism's physiological environment contains substantial concentrations of both of these biomolecules, which are in charge of controlling genetic traits and biological as well as chemical processes, and interactions of 2D materials with them become inevitable upon entering the cellular environment, thereby making them soft targets for toxic interactions.

2. NANOTOXICITY OF 2D MATERIALS TOWARD NUCLEIC ACIDS

The possibility of 2D material-mediated gene transfection involves interaction between them without disturbing the structure of nucleic acids, and a better understanding and visualization of the molecular-level interactions can be achieved by employing computational techniques. Dynamical methods such as classical and ab initio molecular dynamics simulations would certainly be the preferred *modus operandi* in this regard. However, ab initio molecular dynamics (AIMD) simulations suffer from the limitations of system size along with the requirement of massive computational memory and time. Consequently, classical MD simulations appear to be the best alternative to tackle such situations. During the past few years, several simulation strategies have been designed to investigate the nanotoxic effects of the state-of-the-art 2D materials on various types of nucleic acids, namely, single-stranded DNA (ssDNA), double-stranded DNA (dsDNA), RNA, and guanine-quadruplexes (GQ), among others. These nucleic acids differ from each other in their secondary structures and folding patterns. The usual course of these studies progresses via studying the adsorption of nucleic acids, followed by tracking the temporal evolution of the structural characteristics of the nucleic acids, which directly provides evidence for the destacking of nucleobases and depletion of Watson−Crick (WC) and/or Hoogsteen (HS) H-bonding. The structural analyses are often complemented by deducing the underlying energetics, which is, in particular, an indirect way to shed light on the molecular-level basis for the structural

https://doi.org/10.1021/acsphyschemau.3c00053
ACS Phys. Chem Au 2024, 4, 97−121

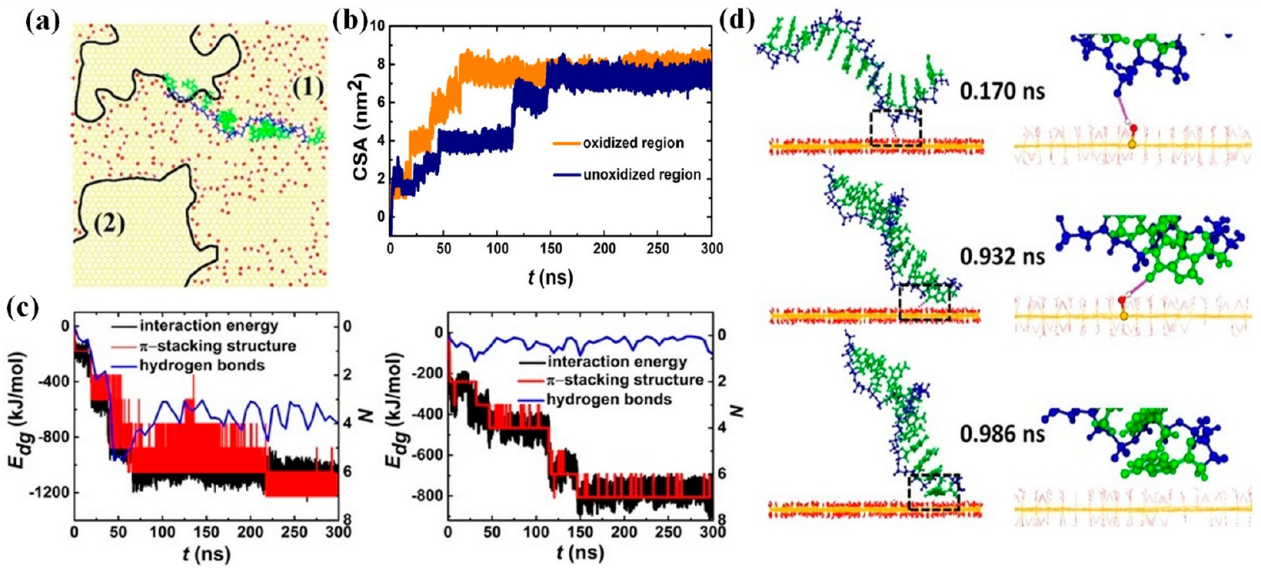

Figure 1. (a) Oxidized (1) and pristine (2) domains of a graphene sheet along with an ssDNA adsorbed. (b) Contact surface area (CSA) and (c) interaction energy, number of H-bonds, and number of $\pi-\pi$ stacking contacts for the adsorption of the ssDNA on oxidized and unoxidized graphene. (d) Snapshots representing a H-bond formed between oxidized graphene with the phosphate backbone and a $\pi-\pi$ stacking contact with the nucleobase. Reproduced with permission from ref 56, copyright 2017 Wiley-VCH Verlag GmbH & Co. KGaA, Weinheim.

alteration of nucleic acids. During the past decade, quite a lot of 2D materials have been subjected to computational screening employing MD simulations for evaluating their toxic effects on the structure of nucleic acids, and the following section addresses key contributions in this realm. For the sake of better understanding of the reader, specific nucleic acids have been chosen followed by the discussion of how they behave upon interaction with the 2D materials.

2.1. Single-Stranded DNA (ssDNA)

ssDNA is the simplest nucleic acid consisting of a single polynucleotide strand where the nucleobases are slip-stacked on each other, and the slippage during their stacking results in turns.[52] Naturally, a single-stranded DNA can be found in class II viruses such as *Parvoviridae* while it can be artificially produced by rapidly cooling a heat-denatured dsDNA, where heating causes the strands to separate and the rapid cooling prevents them from recombination.[53] The sole strand of ssDNA is not noncovalently bonded to any other biomolecular species and therefore is much more susceptible toward interaction with foreign substances. One of the first investigations concerning the adsorption of ssDNA on graphene and graphene oxide was performed by Zeng et al.[54,55] They identified the presence of both H-bonds between nucleotide residues and the hydroxyl and epoxy groups of graphene oxide as well as $\pi-\pi$ stacking between aromatic nucleobases and aromatic rings of the 2D material, as opposed to only $\pi-\pi$ stacking interactions in the case of pristine graphene. dsDNA, on the other hand, was adsorbed much weakly compared to ssDNA, presumably due to the compact nature of the double helical structure which provided lesser exposure to the individual nucleobases.[54] Xu et al. thoroughly studied the adsorption of ssDNA on a graphene sheet which had both pristine and oxidized domains (Figure 1(a)).[56] ssDNA was observed to be completely adsorbed (Figure 1(b)) much faster (~70 ns) on the oxidized section of the 2D material while adsorption on the unoxidized section was somewhat delayed (~150 ns), primarily due to the dynamic cooperation of H-bonds with $\pi-\pi$ stacking interactions in case of the oxidized domain of graphene (Figure 1(c)). This effect was also manifested through the DNA-material interaction energy which, in the case of oxidized graphene, was found to be much higher as compared to the unoxidized section (Figure 1(c)). However, the DNA-graphene π-stacking interactions were formed at the expense of inter-residue $\pi-\pi$ stacking interactions between the nucleobases, thereby disrupting the relative spatial native arrangements of the nucleobases in the ssDNA (Figure 1(d)). Ranganathan et al. investigated the adsorption of different polynucleotide ssDNA of various lengths using experiment-calibrated classical MD force-field parameters.[57] They revealed that the shorter the size of the ssDNA, the greater is the extent of structural disruption from the native state, since the number of nucleobases is not sufficient to maintain their self-stacking. It is worthwhile to mention that in MD simulations interaction energies are calculated through summing up the total electrostatic and van der Waals (vdW) interaction energies between two different molecular entities. The interaction energy is dynamic since it reveals even if there are small changes in the adsorbed molecular conformations on each other and also considers the screening effect of solvent.

Since graphene and graphene oxide significantly perturb the internal structure of ssDNA, other newly synthesized materials could be used instead of GBMs. However, a direct comparison with graphene was necessary to judge whether the disrupting effects of graphene are prevalent even in other materials. To this regard, the adsorption of a model ssDNA was studied on *h*2D-C_2N, pristine graphene, and *h*-BN (Figure 2(a,b)).[58] It was observed that for graphene and *h*-BN, DNA fluctuation occurs initially for only a few hundreds of picoseconds followed by rapid adsorption while for *h*2D-C_2N, the adsorption was significantly delayed. For C_2N and graphene, there was a stepwise increase in the number of contacts during adsorption while in the case of *h*-BN, ssDNA adsorption was exceedingly fast (Figure 2(e)). Similarly, the interaction energies between ssDNA and 2D materials showed a rapid decrease during adsorption, the trend being *h*-BN > graphene

https://doi.org/10.1021/acsphyschemau.3c00053
ACS Phys. Chem Au 2024, 4, 97−121

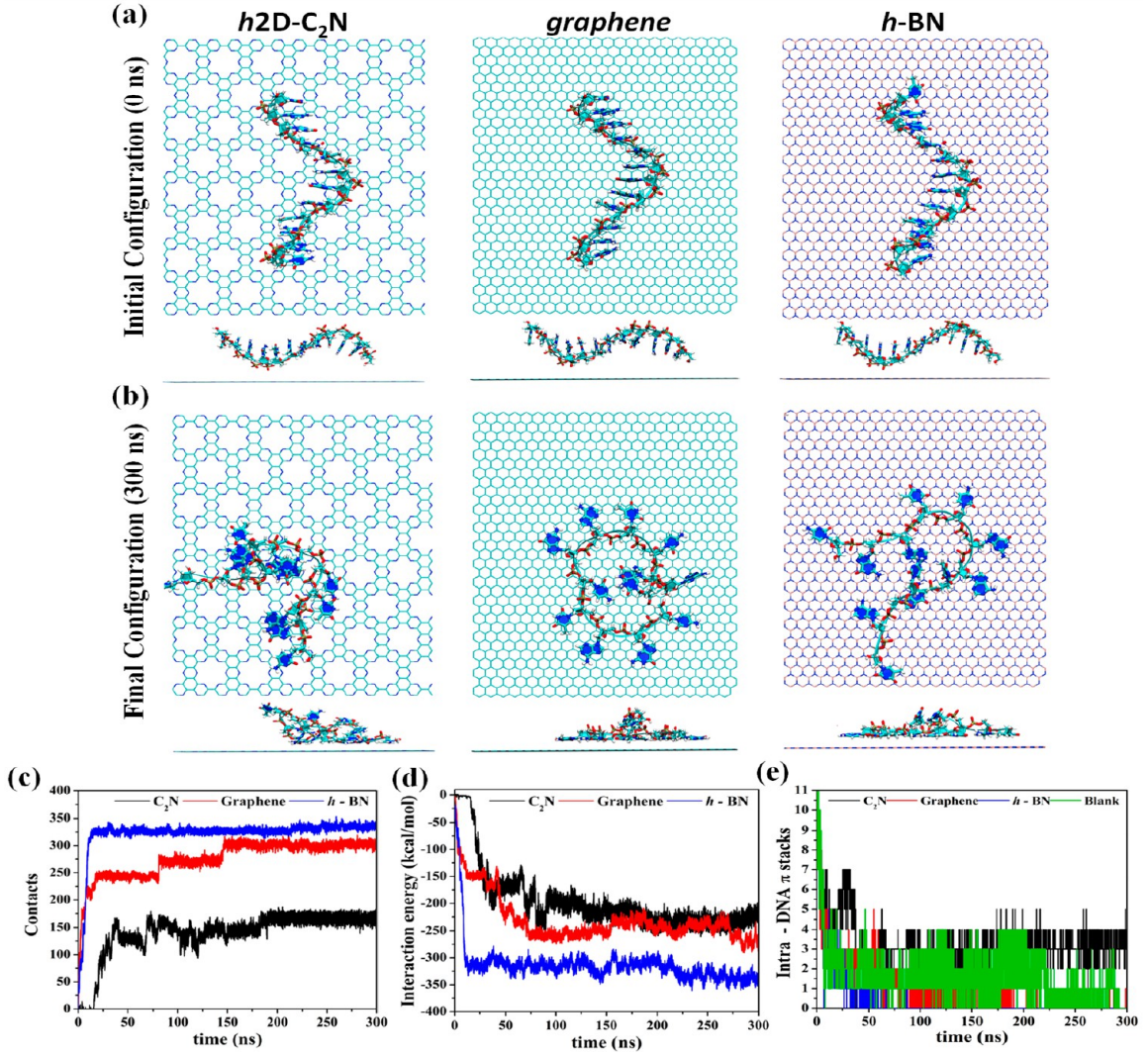

Figure 2. Snapshots of the (a) initial and (b) final configurations of ssDNA adsorption on C_2N, graphene, and h-BN. Time evolution of dynamical quantities characterizing the adsorption and structural evolution of ssDNA on 2D materials: (c) number of contacts, (d) total interaction energy between ssDNA and materials, and (e) intra-ssDNA sequential $\pi-\pi$ stacking contacts. Reprinted with permission from ref 58, copyright 2020 Royal Society of Chemistry.

≥ C_2N (Figure 2(d)). Decomposition of the interaction energies into van der Waals (vdW) and electrostatic components revealed that, during adsorption on C_2N, the increase in interaction energies has nearly equal contributions from both types while for graphene/*h*-BN, vdW interaction was the sole/predominant contributor. For *h*2D-C_2N, 2−3 H-bonds were formed between ssDNA and the material, and therefore a significant share of the electrostatic interaction energy could be attributed to hydrogen bonding. As discussed earlier, graphene and *h*-BN did not form any H-bonds due to the absence of any long-range polarity. Initial structure of the ssDNA contained 11 $\pi-\pi$ stacking contacts, while during the adsorption of graphene and *h*-BN, all the π-stacking contacts were lost, thereby completely disrupting their native state. On the other hand, even after ∼300 ns of adsorption simulation on C_2N, 4−5 inter-residue π-stacking native contacts were maintained (Figure 2(e)), which clearly suggested that C_2N is a better candidate for the preservation of ssDNA.

Although C_2N had been identified as a better adsorbent of ssDNA, the nature of adsorption is likely to be dependent on the polynucleotide sequence.[59−61] We studied the adsorption of four different ssDNA on C_2N, each consisting of 12 nucleotides, corresponding to poly A, G, C, and T, respectively.[62] Both parallel and perpendicular orientations of the ssDNA on C_2N were considered; however, both of them produced a similar perpendicular adsorbed structure, suggesting that the outcome of adsorption is independent of initial orientation. The structure of C_2N consists of a 2D array of aromatic rings, albeit intervened by pores (Figure 3(a)). In addition, each of these pores is surrounded by six electronegative nitrogen atoms, and therefore, the sugar−phosphate backbone and the nucleobases of ssDNA can interact with C_2N through hydrogen-bonding interactions. Three different stages of adsorption were identified, namely, anchoring, adsorption, and reorganization. In fact, for the adsorption of ssDNA on any 2D material surface, these three stages of adsorption existed. After a few nanoseconds of the adsorption simulations (Figure 3(b)), ssDNA comes close to C_2N and makes the first contact through $\pi-\pi$ stacking of a terminal nucleobase (Figure 3(c)). This residue acts as an "anchor" to the surface and remains conformationally locked throughout the simulation. After that, different segments of the ssDNA got sequentially adsorbed

https://doi.org/10.1021/acsphyschemau.3c00053
ACS Phys. Chem Au 2024, 4, 97−121

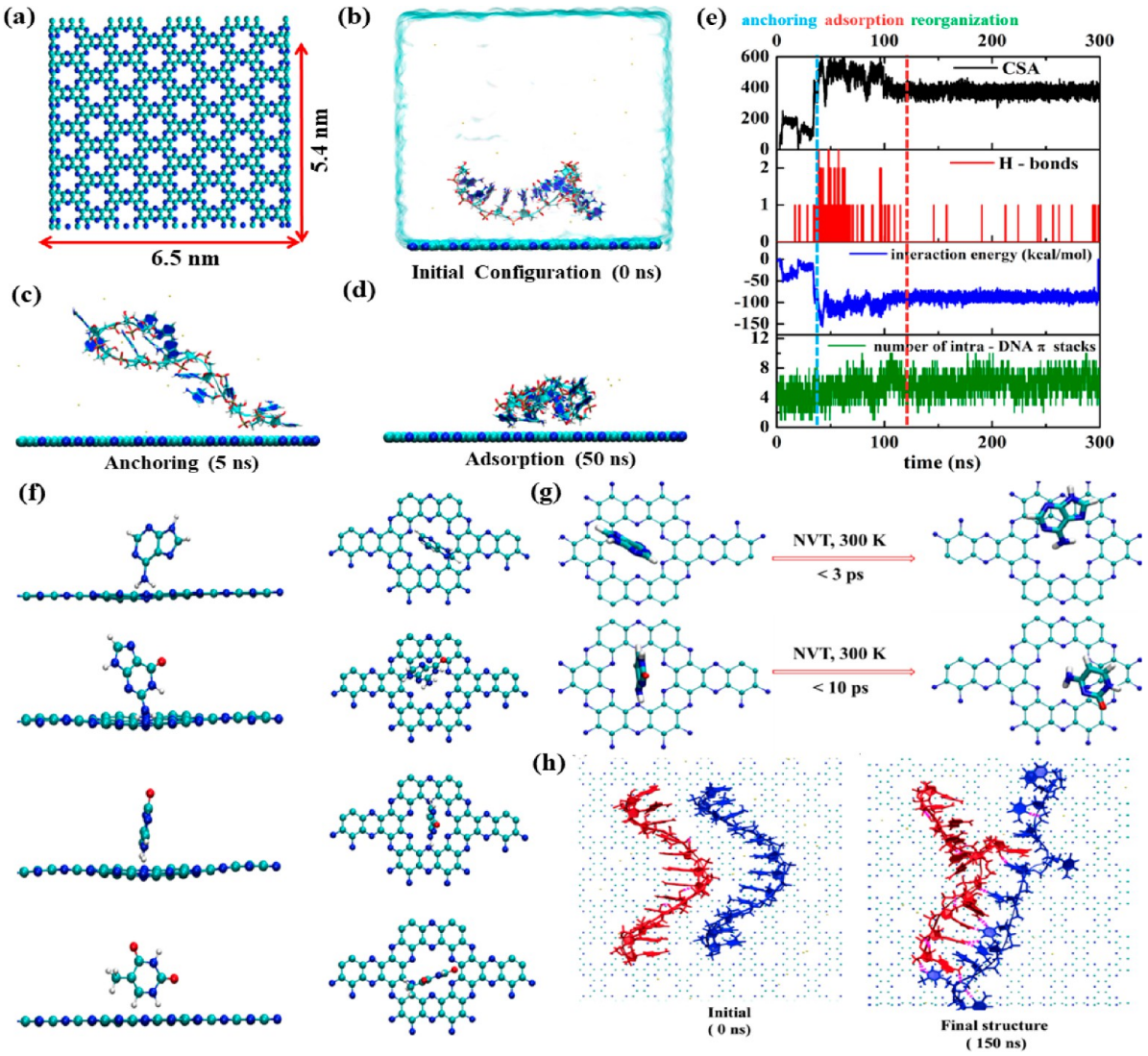

Figure 3. (a) C_2N sheet considered for the adsorption of ssDNA. Different stages of adsorption of ssDNA on C_2N: (b) initial structure, (c) anchoring, and (d) adsorption. (e) Dynamical quantities related to adsorption of poly$(A)_{12}$ on C_2N: contact surface area, interaction energy with C_2N, number of ssDNA-material H-bonds, and intra-ssDNA $\pi-\pi$ stacks. (f) DFT optimized structures of nucleobases on C_2N. (g) Snapshots from ab initio MD simulations of adenine and cytosine on C_2N. (h) Initial and final structures from the simulations of two separate ssDNA over C_2N forming a quasi-double-stranded DNA. Reprinted with permission from ref 62, copyright 2018 American Chemical Society.

(Figure 3(d)), which was realized in terms of a sharp increase in the number of contacts, contact surface area, interaction energy, and number of surface-DNA H-bonds (Figure 3(e)) while the intra-ssDNA native $\pi-\pi$ stacking contacts significantly decrease. However, after the completion of adsorption, the ssDNA experienced reorganization, being characterized by the decrease in the number of H-bonds with a simultaneous increase in intra-ssDNA $\pi-\pi$ stacking interactions. This reorganization occurred to maintain the intra-ssDNA bonding while keeping the adsorption energy on the surface nearly intact, thereby attaining a configuration in phase space where inter-residue stacking as well as interaction with C_2N is optimum (Figure 3(e)). The same situation was observed for all four polynucleotides; however, they differed in the extent of reorganization. Even if the nucleobases reorganized to form their native stacks, the interaction between the nucleobases and the 2D material could be preserved by hydrogen bonds with the nitrogen atoms surrounding the pore. This observation was adequately supported by DFT calculations, which showed that the most stable adsorbed geometry of all four nucleobases were perpendicular conformations with respect to the material plane (Figure 3(f)). To include temperature effects, the DFT optimized structures were further subject to AIMD simulations, producing a somewhat title-perpendicular geometry of the nucleobases, where there is a subtle trade-off between $\pi-\pi$ stacking with the pyrazine rings of C_2N, while maintaining H-bonding with pore nitrogen atoms (Figure 3(g)). The adsorbed state was relatively elongated compared to that found in water, characterized by a higher mean radius of gyration in an adsorbed state ($\langle R_g \rangle$). It was attributed to the presence of surface which interacts with ssDNA, providing a template for adsorption and preventing hydrophobic compaction. For poly A and poly G, the mean number of stacking contacts in the adsorbed state was greater compared to a free state while the situation for poly C and poly T was exactly the opposite. Adenine (A) and guanine (G), consisting of two aromatic rings, undergo a greater extent of reorganization owing to enhanced capability of $\pi-\pi$ stacking

https://doi.org/10.1021/acsphyschemau.3c00053
ACS Phys. Chem Au 2024, 4, 97−121

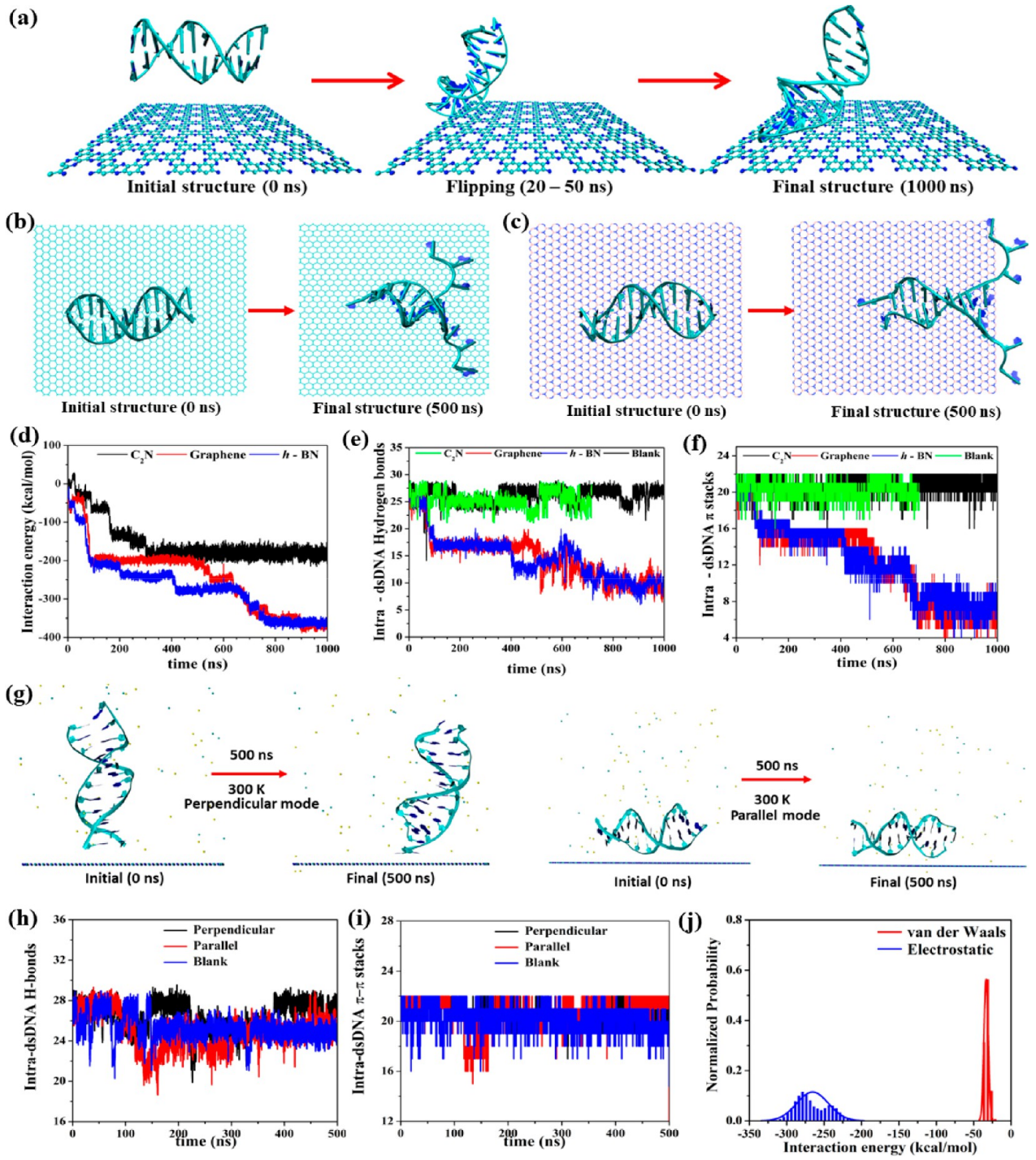

Figure 4. Snapshots representing the initial and final structures for dsDNA adsorption on (a) C_2N, (b) graphene, and (c) h-BN. Dynamical quantities for the adsorption of dsDNA and its structure: (d) interaction energy between dsDNA and 2D materials, (e) intra-dsDNA H-bonds, and (f) $\pi-\pi$ stacking contacts. Reproduced with permission from ref 58, copyright 2020 Royal Society of Chemistry. (g) Snapshots corresponding to the initial and final configurations of perpendicular and parallel modes of dsDNA on g-C_3N_4 and its structural properties: (h) intra-dsDNA H-bonds and (i) $\pi-\pi$ stacking contacts. (j) Probability distribution of the average vdW and electrostatic interaction energies between dsDNA and g-C_3N_4. Reproduced with permission from ref 64, copyright 2020 Wiley.

while cytosine (C) and thymine (T), having only one aromatic ring, show a rather smaller inclination toward the same.[63] As a whole, the native structure of ssDNA was not much perturbed, and most of the native stacking contacts remained intact. The non-nanotoxicity of C_2N toward ssDNA was further demonstrated by considering the possibility of winding two complementary ssDNA molecules poly-A and poly-T, placed antiparallelly with respect to each other on C_2N surface (Figure 3(h)). Within only a few nanoseconds, the ssDNA strands formed the first H-bond between them, followed by a rapid increase in the number of contacts and interstrand H-bonds, resulting in Watson−Crick H-bonding between complementary sets of nucleobases (Figure 3(h)). However, even after many attempts on graphene and *h*-BN, no such

https://doi.org/10.1021/acsphyschemau.3c00053
ACS Phys. Chem Au 2024, 4, 97−121

event was observed due to the enhanced stacking tendency of the aromatic rings of these materials with the nucleobases in conjunction with the unavailability of alternative modes of binding and disruption of the native arrangement of the nucleotides.

A nitrogen-doped 2D GBM similar to C_2N that has gained immense attention in recent years is graphitic carbon nitride (g-C_3N_4). Inspired by the success of C_2N in adsorbing nucleic acids, we performed adsorption simulations with g-C_3N_4 and ssDNA.[64] It was revealed that the ssDNA adsorbed on g-C_3N_4 loses most of its primary stacking contacts unlike on C_2N, and most of the nucleobases form $\pi-\pi$ stacking contacts with the material. However, the structural deviation from the native state was observed to be lesser compared to that observed in case of graphene and *h*-BN while being higher than C_2N. Evaluation of the interaction energies suggested that for both C_2N and C_3N_4, electrostatic and van der Waals interaction energies build up the total interaction energy; however, the contribution from electrostatics was predominant in C_2N, while the van der Waals interaction energy predominates for C_3N_4. It is worthwhile to mention that classical MD simulations recognize the $\pi-\pi$ stacking interactions in terms of van der Waals (vdW) energies only. Therefore, whenever $\pi-\pi$ stacking interactions are mentioned, the reader is requested to recall the origin of such interactions. Practically, $\pi-\pi$ stacking interactions refer to a particular geometry of the interaction between molecular units through vdW forces. When a nucleic acid molecule interacts with a polar 2D material, both electrostatic and vdW interaction energies are built up. If the long-range electrostatic interactions combined with the H-bonding energies dominate over the vdW interactions (e.g., in C_2N), the nucleic acid molecule can reorganize itself and regain the initially lost native $\pi-\pi$ stacking contacts while maintaining the overall adsorption energy; however, in an opposite scenario (e.g., in C_3N_4), desorption of nucleobases from the material leads to significant loss in interaction energy, which in turn, reduces the probability of nucleic acid reorganization.[64] Nevertheless, the relative magnitude of the vdW and electrostatic energies depends on both the nature of the 2D material as well as the nucleic acid, and therefore, different nucleic acids of various polarities can result in different outcomes on a specific 2D material. For nonpolar graphene and locally polar *h*-BN, the contribution from electrostatic interactions was either absent or negligible, and therefore, maximum distortion of nucleic acids was observed on these materials.

2.2. Double-Stranded DNA (dsDNA)

dsDNA molecules are ubiquitous in cellular environments, and it is expected that nanomaterials entering a physiological environment would interact with them.[7,8,23] Although the computational investigations aimed to decipher the interactions between dsDNA and carbon nanotubes have existed even before graphene, the interactions among dsDNA and 2D materials have been studied afterward.[65−68] From a molecular point of view, both carbon nanotubes and graphene share fundamentally similar structures, both consisting of uncharged aromatic rings; however, the shapes of these low-dimensional materials are strikingly different, which may affect the dynamics of the adsorbed nucleic acids. Graphene and other 2D materials are essentially flat, while nanotubes have a barrel-shaped structure, and they possess a certain curvature. Johnson et al. pointed out that the single-walled carbon nanotubes (SWCNTs) induce DNA molecules to undergo a curvature-induced spontaneous conformational change that enables the hybrid to self-assemble via the $\pi-\pi$ stacking interaction between the nucleobases and SWCNT outer surface.[65] DNAs have been observed to spontaneously wrap around the SWCNT within a few nanoseconds, and the native spatial arrangements of the nucleobases were completely disrupted. However, for graphene and other 2D materials, the nature of nucleic acid adsorption is expected to follow a different mechanism. Few of the initial works involving MD simulations of dsDNA with graphene and graphene oxide were performed by Chen et al. and Zeng et al, where they confirmed complete adsorption of the dsDNA on both surfaces, the interaction being dominated by vdW interactions in case of the former while having an additional contribution from H-bonding and electrostatics for the latter.[54,55] Although these studies shed light on the mechanism of adsorption, no comment was made on the time evolution of the structure of the dsDNA molecule. We compared the structural evolution of a model double helical DNA, on both graphene, *h*-BN, and C_2N.[58] The latter was chosen owing to its remarkable performance toward the structural preservation of ssDNA.[62] Figures 4(a-c) shows the initial and final structures of the dsDNA on these three 2D materials. From Figure 4(a), it is evident that a parallelly placed dsDNA on the surface undergoes flipping and becomes perpendicular. On the other hand, on both graphene and *h*-BN, the initial parallel orientation remained unaffected throughout the simulations. For each of the materials there was stepwise decrease in interaction energies during adsorption which followed the order: *h*-BN ≈ graphene ≫ C_2N (Figure 4(d)). Further decomposition of the C_2N-dsDNA interaction energy revealed that the contribution of the electrostatic energies was nearly double that of the van der Waals interactions. In the absence of the 2D materials, the dsDNA was stable at 300 K, characterized by an average of 26 WC bonds (Figure 4(e)) and nearly 22 stacking contacts (Figure 4(f)). However, even after adsorption on C_2N, both of these structural quantities remained similar, whereas on graphene and h-BN, continuous unzipping of the two strands was observed via successive cleavage of WC H-bonds and simultaneous loss of intrastrand stacking contacts, beginning with the anchored terminal base pair and propagating inward. Indeed, the driving force for such structural disruption came from the stability gained by the nucleotide residues through π-stacking with surfaces. Nonetheless, we did not observe complete unzipping of the DNA, and the adsorption was comparatively slower than ssDNA. Therefore, it might be speculated that unzipping would be complete at longer time scales. Such unzipping and structural disruption has also been observed by Hughes et al. for an adenosine-binding DNA aptamer on graphene, while Zhou and co-workers observed structural preservation of a dsDNA on C_2N.[69,70] Additionally, C_2N was observed to adsorb 11-mer of a less stable dsDNA containing 3 pairs of complementary unnatural bases (UBPs) d5SICS and dNaM without perturbing the intra-DNA interactions and H-bonding, while on both graphene and *h*-BN, the nucleobases (both natural and unnatural) underwent immediate adsorption on the 2D materials, thereby disrupting the interactions between the two strands.[58,71] In a nutshell, C_2N was capable of adsorbing dsDNA through both long-range electrostatics and H-bonding along with vdW interactions without hampering the native state.

https://doi.org/10.1021/acsphyschemau.3c00053
ACS Phys. Chem Au 2024, 4, 97−121

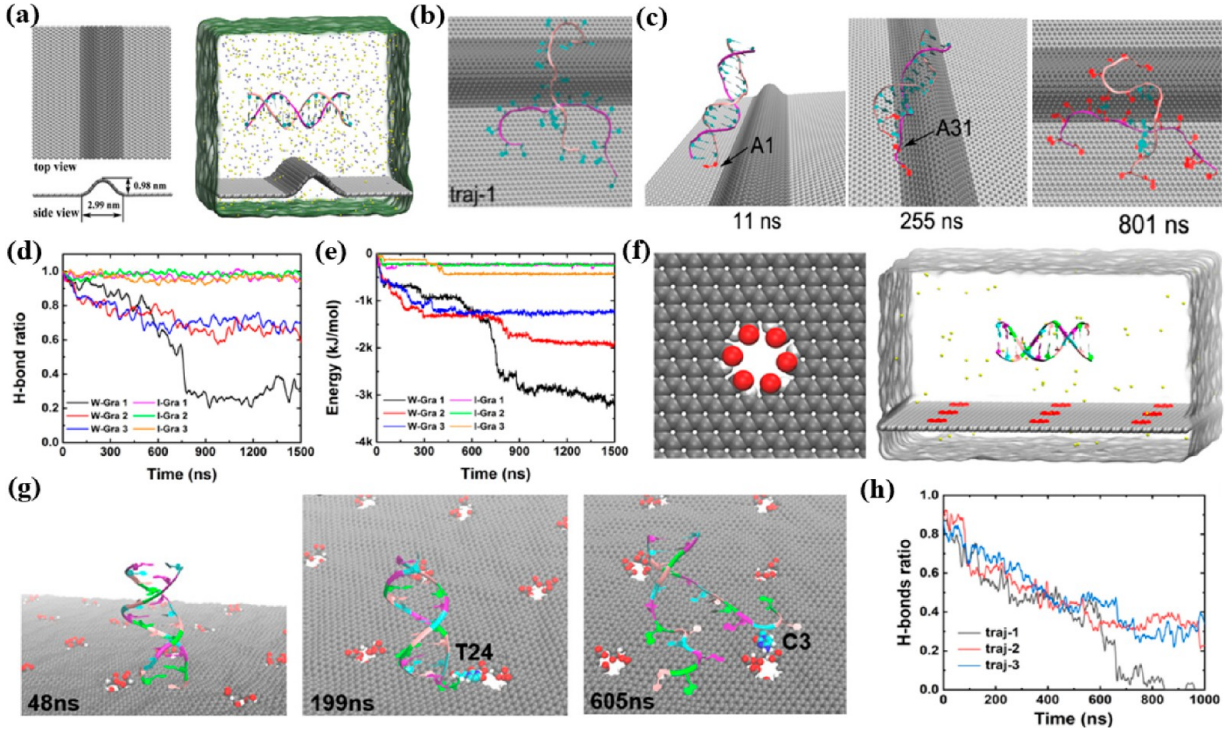

Figure 5. (a) Initial and (b) final structure and (c) snapshots representing the mechanism of "zipper-like unwinding" of dsDNA on wrinkled graphene. Time evolution of (d) ratio of H-bonds of dsDNA during adsorption on wrinkled graphene with those observed in a blank simulation and (e) dsDNA-wrinkled graphene van der Waals interaction energy. Reprinted with permission from ref 80, copyright 2020 American Chemical Society. (f) Initial structure and (g) snapshots representing the mechanism of unwinding of a dsDNA on defective graphene. (h) Ratio of H-bonds during adsorption on defective graphene. Reprinted with permission from ref 81, copyright 2021 American Chemical Society.

Further, the adsorption of a dsDNA with g-C_3N_4 was studied in both parallel and perpendicular initial orientations.[64] Contrary to C_2N, dsDNA did not undergo parallel-to-perpendicular transition (Figure 4(g)), and it could be speculated that the adsorption affinity on g-C_3N_4 was somewhat higher compared to that on C_2N, thereby not allowing the dsDNA to undergo flipping. The structural integrity of the dsDNA was intact in both modes of adsorption, as suggested by the time evolutions of the interstrand WC H-bonds (Figure 4(h)) and the intrastrand $\pi-\pi$ stacking interactions (Figure 4(i)). It was revealed that the unperturbed structure of the dsDNA on g-C_3N_4 resulted due to its much higher electrostatic interactions compared to vdW interactions (Figure 4(j)), thereby allowing the nucleic acid to interact through long-range interactions, a situation being similar to the adsorption of dsDNA on C_2N.[64]

One of the recent additions to the family of carbon nitride 2D materials is polyaniline C_3N, which has been envisaged to display biotechnological application similar to C_2N, g-C_3N_4, and graphene.[72,73] Gu and co-workers studied the interaction between a dsDNA and C_3N following a similar strategy as delineated above.[74] They found that dsDNAs experienced significant unwinding upon adsorption with 20−40% loss in the WC H-bonding between the two nucleic acid strands. The unwound nucleobases experienced twisting from the double-helix and adsorbed on the material through vdW interactions. In fact, the magnitude of the vdW interaction was much higher compared to the electrostatic interaction, which left no other option for the dsDNA but to interact via adsorption of nucleobases, thereby partially disrupting the double-helix. Evidently, nitrogen-containing graphitic 2D materials significantly differed in their interactions with DNAs, and the possibility of structural disruption depended on the relative magnitude of the vdW and electrostatic interactions, a higher magnitude of the former favoring disruption while the latter preferring the preservation of the structure.

Considering noncarbon-based 2D materials other than *h*-BN, recently, Liu et al. and Zhou et al. studied the interaction between a dsDNA with MoS_2 and $MoSe_2$, respectively, both belonging to the transition-metal dichalcogenide (TMDC) family of 2D materials.[75,76] These materials behave similar to each other toward dsDNA, interacting primarily through the vdW interactions via the terminal nucleobases, electrostatic interactions bestowing additional stabilization to the adsorbed molecules. However, the magnitudes of both of these interactions were substantially low when compared with graphene-based 2D materials. Interestingly, they found that the adsorption of the nucleic acid on these materials followed the removal of water molecules present within the immediate vicinity of the terminal nucleobases. Therefore, clearly the interaction strength between the dsDNA and the 2D material was higher compared to the solvation strength with surrounding water molecules. 12-mer and 8-mer dsDNAs were significantly stable on both materials, while a 6-mer dsDNA was more prone to unwinding, probably due to the increase in intra-dsDNA interactions compared to the interaction energy with the 2D materials with an increase in the polynucleotide length. Therefore, molybdenum-based dichalcogenides are non-nanotoxic especially toward DNAs having longer length, and they might be used for biotechnological purposes. The behavior of phosphorene toward dsDNA was found to be similar to those of TMDCs through combined experimental and simulation studies of Zhou and co-workers.[77] Phosphorene as well did not perturb

https://doi.org/10.1021/acsphyschemau.3c00053
ACS Phys. Chem Au 2024, 4, 97−121

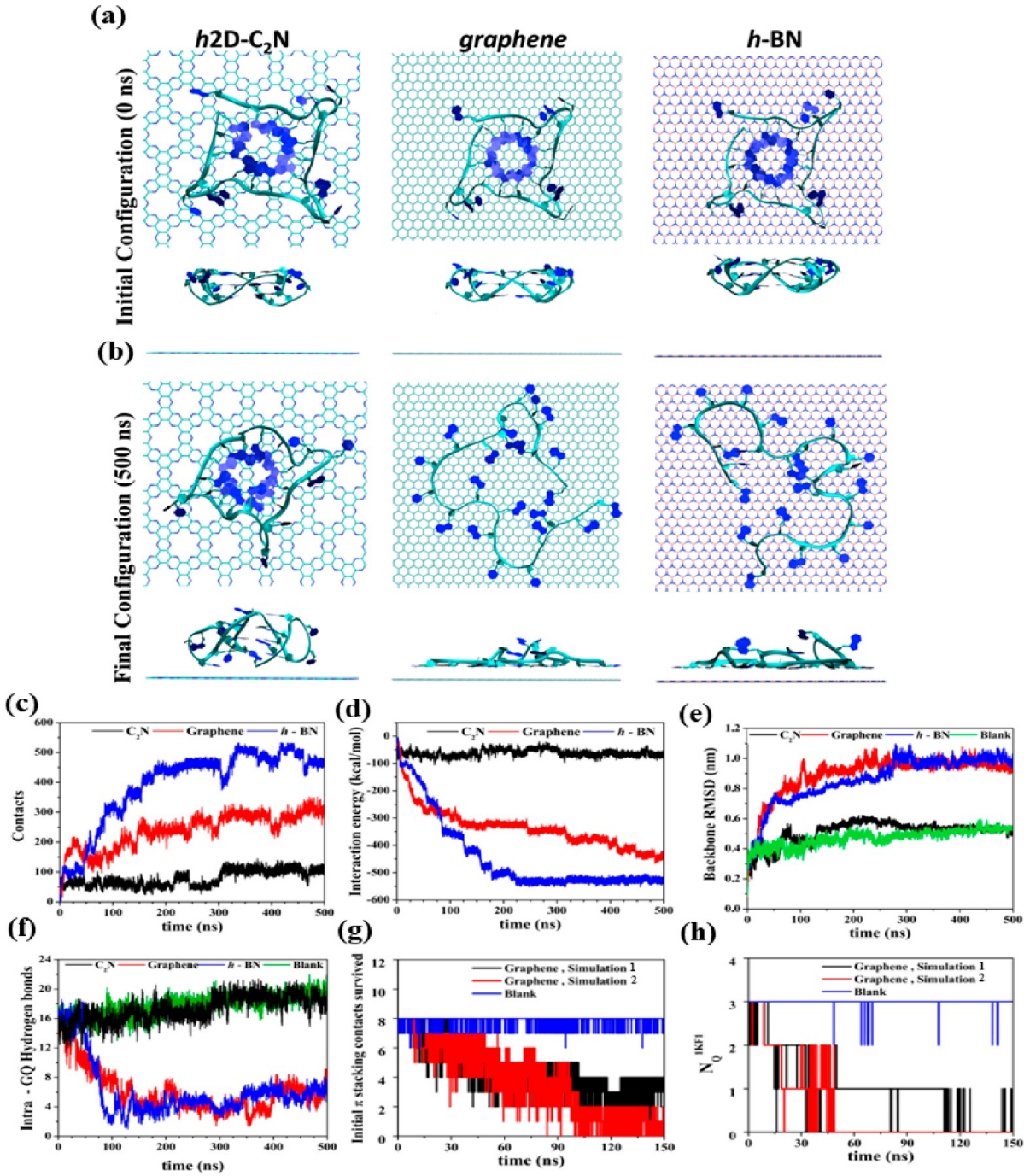

Figure 6. Snapshots representing the (a) initial and (b) final configurations of GQ on C_2N, graphene, and h-BN, respectively. Dynamic properties characterizing the adsorption and structural evolution of a GQ on 2D materials: (c) number of contacts and (d) interaction energy between the GQ and the material, (e) backbone RMSD, (f) intra-GQ H-bonds, (g) intra-GQ $\pi-\pi$ stacking contacts between successive quartets, and (h) number of survived quartets. Reproduced with permission from ref 58, copyright 2020 Royal Society of Chemistry.

the secondary structure and WC H-bonds of dsDNA, and they ascribed the non-nanotoxic effect of phosphorene to the lower interaction energy with the 2D material, which did not surpass the stabilization gained through the intra-DNA interactions. It is worthwhile to mention that the $\pi-\pi$ stacking type of interactions are essentially absent in the case of both TMDCs and phosphorene, due to their nonaromatic nature, undulated structures, and inherent inability to form stacking contacts.

Till now we have discussed the effect of pristine forms of 2D materials on dsDNA; however, under experimental conditions, these materials usually contain wrinkles and defects. Wrinkles are ubiquitous and produced primarily through thermal vibrations and difficult to avoid during the preparation of 2D materials.[78,79] To deduce the effect of large wrinkles on the nanotoxicity of 2D materials, Zhou and co-workers studied the adsorption of a dsDNA on a graphene sheet containing a large wrinkle (Figure 5(a)).[80] It was found that, whenever the dsDNA was adsorbed on the flat section of graphene, the terminal base pairs were unwound, as also reported by us.[58,62] Contrarily, if the dsDNA was adsorbed on the wrinkled domain of the material, it suffered from nearly complete unwinding (Figure 5(b)). After anchoring, gradually the

https://doi.org/10.1021/acsphyschemau.3c00053
ACS Phys. Chem Au 2024, 4, 97−121

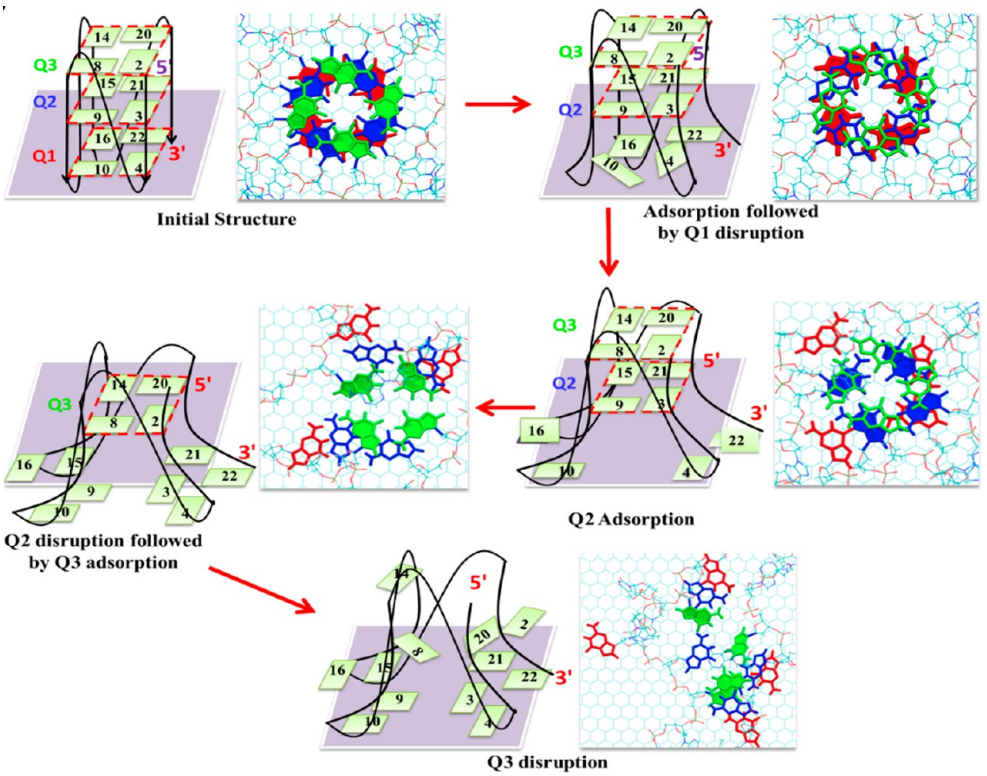

Figure 7. Schematic representation of the hierarchical steps for the "quartet-by-quartet" disruption of human telomeric quadruplex on both graphene and h-BN. Reproduced with permission from ref 58, copyright 2020 Royal Society of Chemistry.

nucleobases get adsorbed on the wrinkled section of graphene (Figure 5(c)) at the expense of H-bonds between the nucleobase pairs (Figure 5(d)), thereby inducing a "zipper-like unfolding". Interestingly, the vdW interaction energy of the dsDNA adsorbed on the wrinkled part of the material was several times higher compared to that of the pristine section (Figure 5(e)), acting as the driving force for the process. Therefore, large wrinkles in materials can indeed induce severe nanotoxicity toward nucleic acids. Similarly, Li et al. studied the adsorption of a dsDNA on defective graphene sheets.[81] Defects on graphene were modeled as a vacancy in the structure, comprising 12 carbon atoms saturated by alternative hydroxyl groups and hydrogen atoms (Figure 5(f)). They observed that the dsDNA adsorption on defective graphene started via the adsorption of the terminal base pairs on a pristine section, followed by interaction with the defective section through H-bonding and electrostatic interactions. The polar defective parts of the material behaved as potential traps, thereby immobilizing the dsDNA through interaction with the terminal part of the nucleic acid. Under this condition, dsDNA underwent a similar unwinding process as observed in the case of wrinkled graphene (Figure 5(g)). The driving force was identified as vdW interactions; however, anchoring of the DNA to the defects behaved as a "pulling force" and held one end of the DNA while the vdW interactions with the pristine sections separated the two strands through H-bond depletion (Figure 5(h)), thereby accelerating the process of unwinding.

2.3. Guanine Quadruplexes (GQ)

Guanine quadruplexes consist of different secondary and tertiary structures as compared to ssDNA and dsDNA and are stabilized through a delicate balance of hydrophobic interactions, π-stacking, and hydrogen-bonding interactions.[82] The structure of quadruplexes consists of two or more guanine quartets, each of them being a cyclic square-planar arrangement of four guanine molecules stabilized by intermolecular Hoogsteen hydrogen-bonding interactions.[83] Two or more such quartet motifs get stacked upon one another during the formation of quadruplexes and are further stabilized by various other forces, such as dehydration of cations and metal-ion binding.[84] Having such a unique structure and arrangement of nucleobases, quadruplexes are prone to interaction with a variety of ligand molecules and surfaces. Several experimental studies have been performed to design sensors based on graphene, graphene oxide, and other 2D materials to detect GQs. Therefore, it is of fundamental interest to investigate whether the structural integrity of these nucleic acids is maintained on 2D materials.

To this regard, the interactions between the three-quartet parallel human telomeric GQ molecule with graphene, *h*-BN, and *h*2D-C_2N (Figure 6(a,b)) were studied.[58] It was found that adsorption on C_2N proceeds through significantly low number of contacts (Figure 6(c)) and interaction energy (Figure 6(d)) while on graphene and *h*-BN, the resulting adsorption was significantly strong, the interaction trend following the order *h*-BN > graphene ≫ C_2N (Figure 6(d)). The structural evolution of GQ showed interesting results. Time evolution of the root-mean-square deviation (RMSD) of nucleic acid backbone (Figure 6(e)) when adsorbed on C_2N was observed to be very similar to that in a blank simulation, as opposed to both graphene and *h*-BN where the RMSD increased rapidly and to an immense extent, suggesting large deviation from the initial structure. This was also supported by the similar time evolution of the intra-GQ H-bonds (Figure 6(f)) in the blank simulations and over C_2N, while being greatly reduced on graphene and *h*-BN. Since the H-bond is

https://doi.org/10.1021/acsphyschemau.3c00053
ACS Phys. Chem Au 2024, 4, 97−121

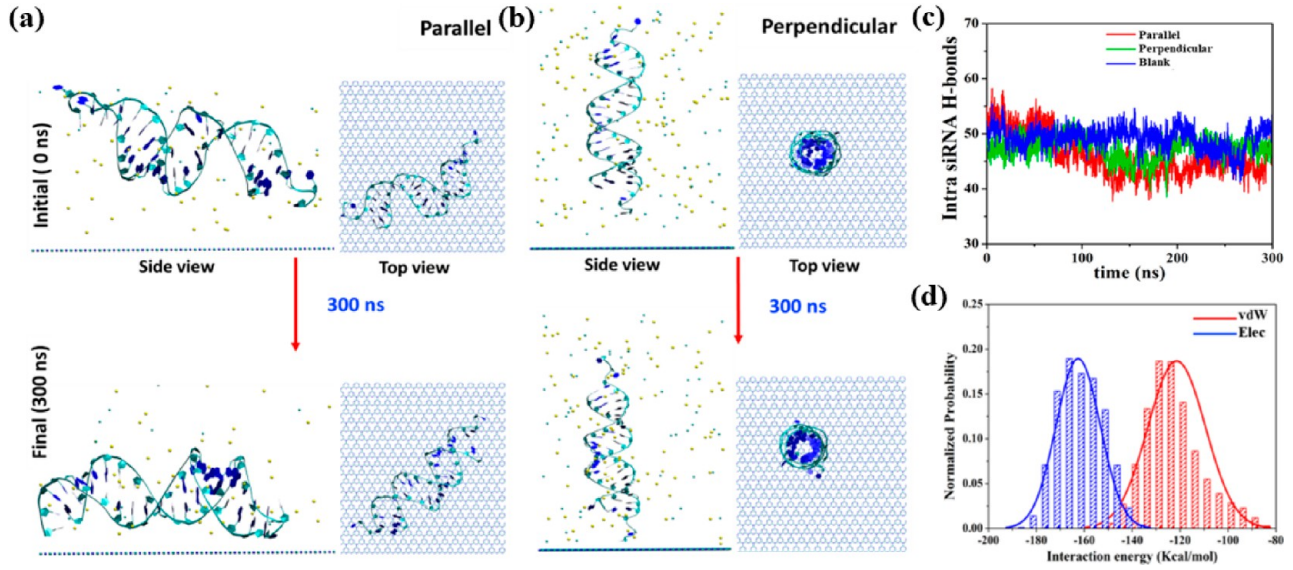

Figure 8. Initial and final configurations for the adsorption of siRNA on g-C_3N_4 having an initially (a) parallel and (b) perpendicular orientation. (c) Time evolution of the intra-RNA hydrogen bonds. (d) Normalized probability distribution of the average vdW and electrostatic interaction energies between the siRNA and g-C_3N_4. Reproduced with permission from ref 64, copyright 2020 Wiley.

one of the key features in stabilizing the quartet structures, it could certainly be predicted that the quartet motifs were disrupted due to the adsorption. We identified two stability parameters, namely, the number of intra-GQ $\pi-\pi$ stacking contacts (Figure 6(g)) and number of quartets (N_Q) survived (Figure 6(h)). The disruption of the GQs on graphene and *h*-BN was observed to follow an "adsorption-induced quartet-by-quartet disruption" mechanism, and Figure 7 provides the schematic representation of the hierarchical steps involved in this mechanism. First, the GQ gets adsorbed on the 2D material (graphene and *h*-BN) via the adsorption of the bottommost quartet motif (Q1) through $\pi-\pi$ stacking of the quartet-forming nucleobases with the 2D material. For graphene and *h*-BN, no stabilizing electrostatic interaction energy is present to allow nucleobase reorganization, and therefore, immediately after adsorption, the quartet structure of Q1 is lost within only 10−20 ns. Therefore, π-stacking with the more hydrophobic graphene and *h*-BN provides the quartet nucleobases a stronger stabilization, which in turn acts as the driving force behind the disruption of Q1. In addition, the nucleobases not involved in quartet formation also get adsorbed on the surface, thereby drastically reducing the structural flexibility of the GQ. These two synchronous events run parallel to each other and weaken the GQ. After the disruption of Q1, the other two quartets Q2 and Q3 also get adsorbed one after another and disrupted in a similar fashion. The sequential disruption of the three quartets was also understood in terms of the steady decrease in the number of intraquartet $\pi-\pi$ stacking contacts. Furthermore, a similar disruption mechanism of several other GQs on both graphene and *h*-BN while being completely stabilized by *h*2D-C_2N suggested that the disruption event was not specific to a specific GQ.

In a later study, the effect of adsorption of GQs on g-C_3N_4 was investigated using a similar simulation protocol.[64] There was an inherent tendency of the GQ to be disrupted upon adsorption on g-C_3N_4 due to the predominance of the vdW interaction energies as compared to the electrostatic interactions. However, the ultimate outcome depends on the initial configuration and adsorbing geometry of the GQ. If the axis of the quartet channel is nearly penpendicular to the plane of the material, the vdW interaction strength is maximum, and therefore the tendency of the nucleobases to form π-stacking with the surface would be higher, thereby inflicting significant perturbation to the structure. However, if the quartet channel axis is tilted with respect to the surface, the formation of π-stacking contacts would be less probable, thereby preserving the GQ structure. Therefore, the toxic effect of g-C_3N_4 toward GQ is lesser compared to graphene and *h*-BN, while being higher than *h*2D-C_2N.

2.4. RNA

Ribonucleic acid (RNA) molecules have gained tremendous attention for their plausible applications in biomedicine, especially therapeutics. Among these applications, antisense therapy is of fundamental interest. It involves delivery of a small interfering RNA (siRNA) double helix by a suitable carrier in an infected cell in order to silence a specific fatal gene.[85−87] 2D nanomaterials have been suggested to be potential carriers of RNA for these purposes.[88,89] However, succeful delivery of the RNA to a specific target would certainly involve the preservation of its structural integrity, and therefore, studying the interactions between RNA and 2D materials has become imperative to contemplate the practical applications of these materials in gene transfection. Chakrabarti and co-workers studied the interactions of a double-stranded RNA and one of its analogues xylonucleic acid (XNA), which contains xylose as the sugar moiety.[90] XNA has an unique structure, adopting a zipper-like double-stranded geometry with a near-orthogonal arrangement of complementary base pairs on opposite strands.[91] It was found that graphene can easily adsorb both XNA and RNA through vdW interactions, displacing the internal arrangements of the nucleobases and cleaving the interstrand H-bonds between complementary base pairs.[90] Clearly, graphene destroys the structure of RNA molecules, behaving as a nanotoxic material. Comparing the interactions between a folded RNA aptamer and graphene oxide as well as *h*-BN, Mashatooki et al. reported that both graphene oxide and *h*-BN were able to disrupt the

https://doi.org/10.1021/acsphyschemau.3c00053
ACS Phys. Chem Au 2024, 4, 97−121

Table 1. Binding Electronic Energies of Free Nucleobases on Graphene, h-BN, and h2D-C_2N, Calculated Using Density Functional Theory, and Binding Free Energies of Free Nucleobases, Calculated from MD Simulations[a]

2D Material	Graphene						*h*-BN			*h*2D-C_2N			MoS_2
Reference	Gowtham et al. (ref 59)		Rao and co-workers (ref 96)	Cho and co-workers (ref 61)			Cho and co-workers (ref 61)			Datta and co-workers (ref 62)			Sadeghi et al. (ref 100)
Method	LDA	MP2	AMBER-FF	LDA	PBE	PBE + vdW	LDA	PBE	PBE + vdW	PBE	PBE + vdW	MD	PBE + vdW
Adenine	−11.3	−21.7	−17.8	−12.7	−1.4	−23.1	−12.9	−1.6	−23.3	−9.7	−20.6	−14.8	−18.0
Guanine	−14.1	−24.7	−19.1	−16.6	−3.2	−27.2	−17.3	−3.5	−27.2	−10.5	−23.0	−16.2	−18.8
Cytosine	−11.3	−18.4	−14.5	−12.9	−3.0	−21.4	−13.6	−3.0	−21.4	−17.6	−27.7	−17.6	−17.7
Thymine	−11.3	−19.1	−16.6	−12.4	−1.8	−21.9	−13.1	−1.8	−21.7	−0.8	−11.5	−13.2	−17.3

[a]Reprinted with permission from ref 59, copyright 2007 The American Physical Society, ref 96, copyright 2009 Wiley, ref 61, copyright 2013 American Chemical Society, ref 62, copyright 2018 American Chemical Society, and ref 100, copyright 2017 Elsevier B.V. Binding energies have been converted from eV per molecule to kcal/mol.

structures of the RNA, *h*-BN cleaving the H-bonds and disrupting the secondary structure faster as compared to graphene oxide, thereby showing a higher degree of nanotoxicity.[92] As a result, it was indeed necessary to explore other biocompatible 2D materials toward RNA molecules. In search for such materials, we studied the adsorption of an siRNA on g-C_3N_4.[64] siRNA is a class of double-stranded noncoding RNA molecules, having 20−25 base pairs and consisting of phosphorylated 5′ and hydroxylated 3′ ends. Two different initial structures were considered where the siRNA is perpendicular and parallel to the material plane (Figure 8(a,b)). The initial orientation of the siRNA did not change upon adsorption onto the surface, and neither did the secondary structure. The parallel and perpendicular forms of the adsorbed siRNA were clearly distinguishable from each other through visual analyses. Detailed analyses revealed that interstrand WC H-bonding (Figure 8(c)), $\pi-\pi$ stacking interactions, and other structural parameters reamined nearly unaltered when compared with a blank simulation. Therefore, g-C_3N_4 could easily be used for the purpose of adsorption of RNAs unlike graphene and *h*-BN. This behavior of g-C_3N_4 was again explained in terms of the predominance of the electrostatic interactions of the nucleic acid with the material over the vdW interactions (Figure 8(d)), an observation similar to that of dsDNA.

2.5. Thermodynamic Considerations

Nanotoxic effects of 2D materials are manifested via chemical modifications of nucleotides and/or through the disruption of the secondary and tertiary structures of the polynucleotides owing to their strong adsorption on the materials. Evaluation of the energetics of such interactions may shed light on the thermodynamic foundation of nanotoxicity. DFT and MD simulations are invaluable computational tools in this regard, since DFT has the capability to track the chemical interactions while MD simulations can be used to deduce the adsorption free energies of large molecular entities in a solvent environment, taking the thermal effects into considerations. In recent years, several research groups have evaluated the binding energies of nucleobases and nucleotides on various 2D materials, and Table 1 lists some of these for graphene, *h*-BN, *h*2D-C_2N, and MoS_2. In DFT, the binding energy is calculated by subtracting the electronic energies of the individual molecular components from the electronic energy of the hybrid system showing binding. It does not include the temperature, solvent, and entropic effects, as opposed to the binding free energies calculated from MD simulations, where all of the above-mentioned effects are taken into consideration. Gowtham et al. calculated the binding energies for these molecules using both periodic DFT within the local density approximation (LDA) and MP2 calculations for nonperiodic molecular systems.[59,93−95] They found that the binding energies follow the order G > A ≈ T ≈ C under LDA and G > A > T > C in case when the MP2/6-311++G(d, p) level of theory is applied. Rao and co-workers used AMBER force fields in vacuum phase to calculate the binding energies which followed the same order as obtained from their isothermal titration calorimetry (ITC) experiments.[96] Cho and co-workers employed local (LDA), semilocal, and van der Waals energy-corrected periodic density-functional theory (PBE + vdW) to show that the magnitudes for different schemes of calculations following the order PBE+vdW > LDA > PBE.[61] While the LDA scheme produced a binding energy trend similar to that (G > A ≈ T ≈ C) obtained by Gowtham et al., the PBE scheme without vdW corrections predicted a different trend: G ≈ C > T > A.[59] Inclusion of the vdW corrections predicted the binding energies to follow the same trend as obtained by Rao et al.[96] Interestingly, the trend and magnitudes of the binding energies obtained by the PBE+vdW scheme corroborated with those found in ITC and single solute adsorption isotherm studies.[96,97] The same trend in binding energies was found for the interactions between *h*-BN and nucleobases, although the magnitudes were higher as compared to graphene.[61] An analogous trend in the binding affinities was also found by Johnson et al. for the adsorption of nucleobases on single-walled carbon nanotubes.[98] They decomposed the enthalpic and entropic parts of the free energies to demonstrate that the solvent and entropic effects were negligible, and the adsorption of the nucleobases was essentially guided by van der Waals interactions. Calculations of the band structures of the nucleobases adsorbed on both graphene and *h*-BN demonstrated that the occupied molecular states of the nucleobases had no band dispersion, suggesting negligible hybridization with the π-states of the graphene and BN.[61] Mulliken charges showed an insignificant charge transfer of less than 0.03e between the nucleobases and the 2D materials.[61] Therefore, the strong adsorption of the nucleobases on graphene and *h*-BN resulted from physisorption rather than having a chemical interaction between them. We calculated the binding energies of the four nucleobases on *h*2D-C_2N which followed the order C > G > A > T, and the magnitudes of binding energies in the PBE + vdW scheme were similar to those observed for graphene and *h*-BN.[62] Free

https://doi.org/10.1021/acsphyschemau.3c00053
ACS Phys. Chem Au 2024, 4, 97−121

energy calculations of the nucleobases on *h*2D-C_2N in vacuum also predicted the same trend, albeit the magnitudes were reduced from the DFT calculated values due to temperature and entropic effects.[62,99] Analysis of the density of states (DOS) of the nucleobase-C_2N hybrids confirmed the minimum electronic perturbation of the nucleobases after adsorption, clearly suggesting the absence of any chemical interaction with the surface. Sadeghi et al. determined the binding energies of the nucleobases on MoS_2 employing vdW corrected periodic DFT, which showed a different trend: G > A > C > T; however, the magnitudes appear to be smaller compared to the above-mentioned 2D materials, presumably due to the absence of $\pi-\pi$ stacking interactions between the nucleobases and nonaromatic MoS_2.[100]

In recent years, 2D materials have been predicted as plausible candidates for nucleic acid delivery vectors. Although experimental methods can determine whether the nucleic acid delivery is possible using 2D materials, MD simulations can be used for the indirect prediction of the same *a priori* to experiments. Such a strategy has been developed and applied in our recent studies where adsorption free energies of nucleic acids have been utilized in conjunction with the Smoluchowski equation to calculate the mean first-passage time of the nucleic acids from the 2D materials.[58,64] The calculated magnitudes of the adsorption free energies for various nucleic acids on *h*2D-C_2N, g-C_3N_4, graphene, and *h*-BN suggest that the free energy penalty for their desorption is significantly higher compared to the energy available due to thermal motions.[58,62,64] An external stimulus would invariably be required to facilitate this purpose, and the spontaneous release of DNAs from an adsorbed state might be considered as a rare event. Consequently, the time scales of occurrences of such events might be in the order of seconds, hours, or days, which are far beyond the accessible time scales of the current state-of-the-art of classical MD simulations. Therefore, we modeled the release of these molecules as diffusion in the presence of a potential $W(z)$ along a reaction coordinate employing the analytical Smoluchowski equation. To develop the necessary theoretical framework, the diffusion of the nucleic acids was assumed to occur in the presence of a potential $W(z)$ along a one-dimensional reaction coordinate, the distance along the z (vertical) axis, in particular. The probability $P(z',t|z,0)$ of finding the particle at a position z' and at time t, knowing that the particle was present at position z at time $t = 0$, where t is prior to the time $t = 0$, can be written in terms of the backward Smoluchowski equation as[58,64]

$$\frac{\partial P(z,t)}{\partial t} = \frac{\partial}{\partial z}\left\{ D(z)e^{-W(z)/kT}\frac{\partial}{\partial z}[e^{-W(z)/kT}P(z,t)]\right\} \quad (1)$$

where $D(z)$ and $W(z)$ are the diffusivity and one-dimensional free energy landscapes, respectively. The time taken for the release ($\tau_{release}$) of the nucleic acids is expressed in terms of the mean first-passage time

$$\tau(z, z_{out}) = \frac{1}{D}\int_{z}^{z_{out}} dz' e^{W(z')/kT} \times \int_{z_{ref}}^{z'} dz'' e^{-W(z'')/kT} \quad (2)$$

where $\tau(z,z_{out})$ is the average time taken for the nucleic acid to travel from an initial position z to the final released state with position z_{out}. z_{ref} is termed as a reflective boundary and D is the diffusion coefficient. The diffusion coefficient D in the above equations is originally position (z)-dependent; however, here we consider it to be constant for an adsorbed structure since small changes in the vertical distance between the 2D material and the nucleic acid do not change the diffusivity appreciably, as long as some residues are adsorbed on the surface. The free energy landscape $W(z)$ was calculated in terms of the one-dimensional potential of mean forces, representing the free energy profiles for adsorption. The instantaneous position of the nucleic acid lied between the two boundaries z_{out} and z_{ref}, i.e., $z_{ref} \leq z \leq z_{out}$. Insertion of the diffusion coefficients and free energy profiles into eq 2 yields the release times for various nucleic acids on different 2D materials, which are listed in Table 2. From the magnitudes of the release times, it can safely be concluded that relatively weakly adsorbed nucleic acids on *h*2D-C_2N and *g*-C_3N_4 can be released at a higher rate; however, for GQs adsorbed on *g*-C_3N_4, a much higher release time is required compared to *h*2D-C_2N. In contrast, for graphene and *h*-BN, the release times were orders of magnitude higher, making them poor platforms for nucleic acid delivery.

Table 2. Estimated Release Times ($\tau_{release}$) of Nucleic Acids (in nanoseconds) from an Adsorbed State on the 2D Surfaces[a]

Type of DNA	2D material	Release time ($\tau_{release}$(ns))
ssDNA	*h*2D-C_2N	1.25×10^{26}
	g-C_3N_4	6.91×10^{31}
	Graphene	1.77×10^{88}
	h-BN	6.63×10^{95}
dsDNA	*h*2D-C_2N	1.11×10^{33}
	g-C_3N_4	4.96×10^{19}
	Graphene	8.30×10^{49}
	h-BN	1.51×10^{46}
GQ	*h*2D-C_2N	1.34×10^{31}
	g-C_3N_4	4.24×10^{66}
	Graphene	1.83×10^{156}
	h-BN	2.41×10^{259}

[a]Reprinted with permission from ref 58, copyright 2020 Royal Society of Chemistry and ref 64, copyright 2020 Wiley.

An important aspect regarding the delivery of nucleic acids from an adsorbed state is the specificity of targeting. It has been reported that biomolecules adsorbed on 2D materials might undergo longitudinal diffusion across the surface activated by thermal motions.[70] The 2D materials used in real experiments are significantly large in their dimensions, and therefore, "crawling" of nucleic acids on the surfaces may lead to loss in specificity during their delivery. Therefore, it is imperative to understand the driving force and material-selectivity for the lateral movement of the DNA molecules. The possibility of lateral translation of adsorbed nucleic acids on 2D materials can be investigated by constructing 2D free energy landscapes for the movement of the biomolecule on the material, which reveals the corrugation in the free energy landscapes encountered during "crawling". We calculated the free energy profiles for the lateral movement of a guanine nucleobase in vacuum on C_2N, taking the projection of the center-of-mass (COM) distance along both x and y axes as the reaction coordinates, as shown in Figure 9(a).[58,101] C_2N contains periodic pores (designated as A, B, and C in Figure 9(a)) surrounded by electronegative nitrogen atoms, where the nucleobases can attach through H-bonding, being simultaneously stabilized by the neighboring aromatic rings through

https://doi.org/10.1021/acsphyschemau.3c00053
ACS Phys. Chem Au 2024, 4, 97−121

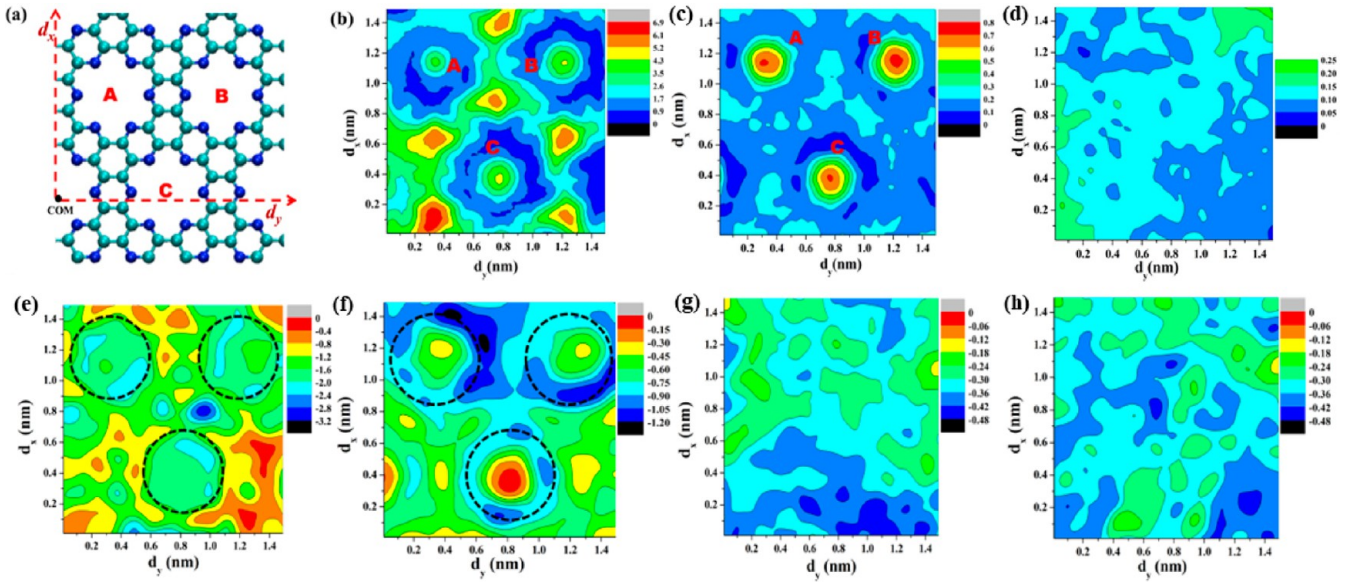

Figure 9. (a) Section of C_2N for which the 2D free-energy profiles are constructed. 2D free energy profiles (in kcal/mol) for the in-place displacement of a guanine molecule adsorbed on (b) C_2N, (c) C_2N without partial charges, and (d) graphene in vacuum. Reprinted with permission from ref 101, copyright 2018 American Chemical Society. Free energy landscapes for the lateral movement of a single mononucleoside deoxyadenosine (dA) on (e) C_2N, (f) C_2N without partial charges, (g) graphene, and (h) h-BN in an aqueous medium. Reproduced with permission from ref 58, copyright 2020 Royal Society of Chemistry.

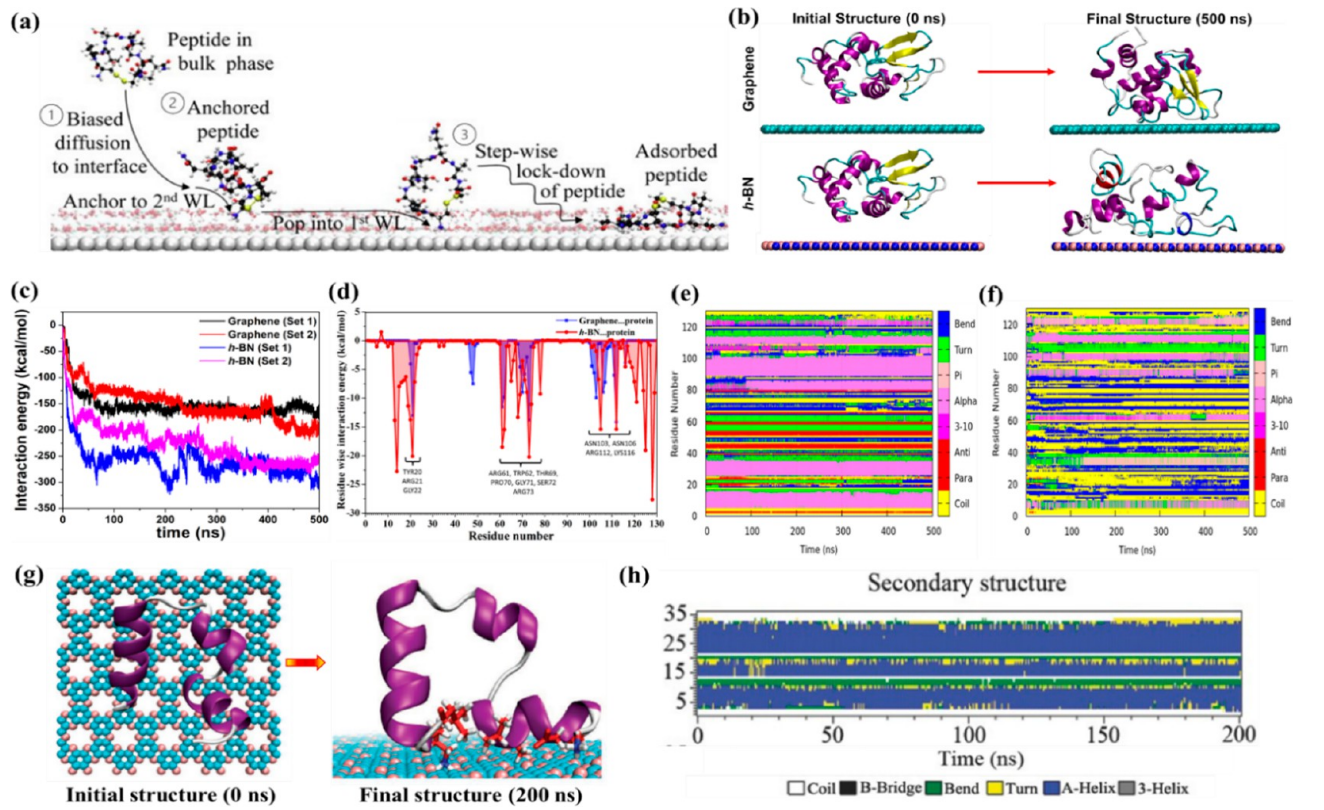

Figure 10. (a) Hierarchical stages of the adsorption of peptides on 2D materials. Reprinted with permission from ref 109, copyright 2014 American Chemical Society. (b) Initial and final structures, (c) interaction energy, (d) residue-wise decomposition of interaction energies, and time evolution of the secondary structure of HEWL adsorbed on (e) graphene and (f) h-BN. Reprinted with permission from ref 117, copyright 2023 American Chemical Society. (g) Initial and final configurations of HP35 protein on h2D-C_2N, and (h) time evolution of the secondary structure. Reprinted with permission from ref 118, copyright 2017 Wiley.

$\pi-\pi$ stacking. However, there are no atoms present just above the pore to interact with the nucleobases. Therefore, nucleobases remain in a low free-energy region beside the pores while encountering a barrier of ~2 kcal/mol (Figure 9(b)). As the molecule moves away from the pore, the free energy progressively decreases and eventually reaches a plateau

https://doi.org/10.1021/acsphyschemau.3c00053
ACS Phys. Chem Au 2024, 4, 97−121

of the landscape having a small free energy barrier of <1 kcal/mol, where the molecules are nearly freely diffusing. After that, another barrier is encountered separating the three porous regions, when the molecule interacts only through $\pi-\pi$ stacking with the aromatic rings but the H-bonds are lost. Interestingly, upon withdrawal of the partial charges, the H-bonding disappears, and the free energy magnitudes are substantially reduced (Figure 9(c)). The only barrier encountered is the one situated on the top of the pore due to the absence of atoms. Therefore, the porous nature and presence of localized polarity in C_2N induce formation of periodic potential energy traps, thereby clamping the nucleobases during their adsorption and preventing lateral motion. However, for graphene (Figure 9(d)), the free energy landscape is nearly uniform due to the presence of symmetric hexagonal rings, which isotropically interact with an adsorbed molecule, making the encountered barriers within the limit of thermal energy and providing ample opportunity for the molecule to move across the surface. Next, we deduced the free energy landscapes in the presence of aqueous medium for a mononucleoside deoxyadenosine (dA) (Figure 9(e-h)).[101] The free energy pattern remained grossly similar in nature; however, the magnitudes of the energies were reduced due to the screening effect of solvent. The maximum free energy barrier encountered was about ∼2.5 kcal/mol compared to ∼6 kcal/mol observed for guanine in vacuum, both being significantly higher than the thermal energy available, and therefore led to immobilization of the nucleobases through H-bonds and/or $\pi-\pi$ stacking interactions. For graphene and *h*-BN, the free energy landscape pattern and magnitude do not change in the presence of water, and nucleic acids are nearly free. Therefore, evidently C_2N appears to be a good alternative compared to graphene and *h*-BN due to the higher specificity of the location of adsorption of single nucleobases and nucleosides on the former.

3. NANOTOXICITY OF 2D MATERIALS TOWARD PROTEINS AND PEPTIDES

The biomedical use of graphene and related 2D materials involves inevitable interaction with amino acid molecules, peptides, and proteins, upon entering the physiological environment, since proteins are one of the more abundant classes of molecules present in the cellular and extracellular environments of living organisms. Classical MD simulations have historically been used to describe the structure, folding-unfolding dynamics, water and small-molecule interactions, secondary structure dynamics, and denaturation of proteins.[102−108] Therefore, with the development of MD parameters for the simulations of 2D systems, classical MD simulation turns out to be the preferred tool to attack the problem of computational evaluation of the nanotoxicity of 2D materials toward proteins and peptides. After realizing the biomedical potential of graphene and related 2D materials, significant efforts have been invested regarding such computational investigations, which in turn have unravelled a great deal of information underlying the interactions between proteins and 2D materials, and some of the important conclusions have been discussed in the following section.

3.1. Interactions between Proteins and Peptides with 2D Materials

One of the first investigations concerning peptides and solid surfaces was performed by Penna and Biggs.[109,110] They identified a three-phase adsorption mechanism, as illustrated by Figure 10 (a): (1) the first stage involves the biased diffusion of the peptide/protein from the solution toward the surface, (2) reversible "anchoring" of the biomolecule via hydrophilic groups of the peptide to the second water layer adjacent to the surface, and (3) a "lockdown" phase, consisting of the slow and stepwise rearrangement of the peptide initiated by the anchor group piercing into the first water layer, along with other hydrophobic and hydrophilic residues. However, these conclusions were based on a limited number of simulations, and generalization of this mechanism required significant modification. Yu et al. proposed that the biased diffusion phase was accompanied by the building up of long-range electrostatic interactions with the highly oriented layers of water molecules near the surface in conjunction with van der Waals and hydrophobic interactions with the material.[111] H-bonding with the water molecules has also been predicted to play important roles during the adsorption of proteins and peptides on solid surfaces. Simulation studies have found that the fundamental nature of adsorption of proteins remains the same on 2D materials, the adsorption strength being controlled by the mutual interactions between the amino acid residues and the materials.[112]

Guo et al. studied the interactions betweeen three proteins having different secondary structures, namely, the WW-domain (β-sheet), BBA protein (mixture of α-helix and β-sheet), and λ-repressor (α-helix) with graphene.[113] Being nonpolar, graphene interacted with the proteins only through van der Waals forces, and there was no electrostatic influence. Upon adsorption, the antiparallel β-sheet secondary structure of the WW-domain remained nearly intact, while the α-helical content of the λ-repressor protein underwent significant perturbation and was either lost or converted to the 3_{10}-helix. In case of the BBA protein, the perturbing effect of the material was significant, destroying most of its α-helical component and significantly affecting the β-sheets. However, the extent of structural perturbation was dependent on the binding orientation of the protein and the residues available for interaction. It was suggested that the rigidity of the β-sheet structures was responsible for the protection from denaturation, while the flexible α-helix was prone to adsorption-induced disruption by graphene. This observation was also complemented by the investigation of the adsorption of Villin Headpiece (HP35) on graphene by Guo et al. employing MD simulations, where they found nearly complete conversion of the α-helix into 3_{10}-helix.[114] Free energy calculations predicted that the adsorption of protein on graphene was highly favorable from an enthalpic point of view, while being slightly disfavored entropically, making the overall free energy favorable for adsorption. Since the nature of amino acid residues controls the extent of adsorption on 2D materials, mutating a protein with one or few amino acids may change the local conformation of the protein. For instance, the immunoglobulin G (IgG) antibody-binding domain of protein G, also known as G_B, easily gets adsorbed on graphene through vdW and $\pi-\pi$ stacking interactions and gets structurally denatured by the material. Wei et al. mutated the strongly interacting Gln32 and Asn35 residues of G_B with weakly adsorbing alanine residues and demonstrated that the sequence-engineered mutated protein did indeed maintain its secondary structure.[115] Therefore, MD simulations also allowed researchers to visualize and study the effect of protein mutations on their adsorption.

https://doi.org/10.1021/acsphyschemau.3c00053
ACS Phys. Chem Au 2024, 4, 97−121

The nanotoxicity of 2D materials toward proteins and peptides, as discussed until now, depends on the nature and population of the amino acid residues, a larger fraction of strongly adsorbing residues enhancing the toxic and disruptive effects while a higher population of weakly interacting amino acids increasing the probability of structural preservation. To fundamentally understand the adsorption behavior, Hughes and Walsh calculated the free energies of all 20 natural amino acids on graphene in the presence of aqueous medium (Table 3), which revealed a few key points:[116] (1) aromatic amino acids (Tyr, Trp, His, and Phe) have high adsorption free energies on graphene, (2) other than the aromatic amino acids, Arg, Asn, Gln, Gly, and Met have significantly high adsorption propensities, (3) the most weakly adsorbing amino acids were Ile, Lys, Pro, Leu, and Val, (4) the size of the side chains has no correlation with the free energies, since large side chains bearing Arg, Gln, and Trp have higher free energies while Gly has significantly strong adsorption on graphene in spite of having the smallest size, (5) weakly adsorbing amino acids can either be hydrophobic (Ile, Leu, and Val) or hydrophilic (Lys), and therefore, hydrophilicity has no correlation with the free energies, and (6) amino acids possessing planar groups (phenyl, indole, guanidium, and amide groups) interact with graphene through $\pi-\pi$ stacking interactions and, therefore, have higher free energies, while those having bulky or strained side chains (Ile, Leu, Val, and Pro) are weakly adsorbing.[116]

Table 3. Free Energies of Adsorption for Natural Amino Acids on Graphene[a]

Amino acid	Free energy of adsorption (kcal/mol)
Ala	−2.49 ± 0.31
Arg	−5.54 ± 0.17
Asn	−3.66 ± 0.65
Asp	−2.01 ± 0.26
Cys	−2.58 ± 0.17
Glu	−2.63 ± 0.22
Gln	−5.21 ± 0.22
Gly	−4.47 ± 0.38
His A	−3.20 ± 0.36
His H	−4.30 ± 0.29
Ile	−0.67 ± 0.19
Leu	−1.72 ± 0.22
Lys	−1.65 ± 0.17
Met	−3.94 ± 0.50
Phe	−3.56 ± 0.36
Pro	−1.72 ± 0.17
Ser	−3.18 ± 0.50
Thr	−2.51 ± 0.24
Trp	−5.11 ± 0.69
Tyr	−4.97 ± 0.26
Val	−1.82 ± 0.26

[a]Reprinted with permission from ref 116, copyright the Royal Society of Chemistry, 2015. The free energies have been converted from kJ/mol to kcal/mol to maintain continuity.

Apart from graphene, the material of interest would certainly be *h*-BN, which has already been shown to interact more strongly with nucleic acids as compared to graphene, destroying their secondary structures, and it is expected that *h*-BN would also behave in a similar manner toward proteins. In this regard, Paul and co-workers have studied the interaction of a model protein hen egg white lysozyme (HEWL), toward both graphene and *h*-BN.[117] It was observed that HEWL was spontaneously adsorbed on both the materials (Figure 10(b)), the interaction energy with *h*-BN being much higher (Figure 10(c)), completely corroborating the trend observed for nucleic acids. Decomposition of the interaction strengths (Figure 10(d)) of an individual residue with the 2D materials reveals that for both materials most of the interacting residues were common with several clusters of residues comprising TYR, ARG, GLY, TRP, and HIS, which have been listed above as strongly interacting residues, and each of these amino acid residues had higher interaction strength with *h*-BN. It was demonstrated that graphene nearly maintained the secondary structure of the protein (Figure 10(e)) while upon adsorption on *h*-BN (Figure 10(f)), the α-helix content was reduced and the β-sheet content of HEWL got completely diminished, an observation opposite of those observed for several proteins on graphene. Therefore, the toxicity of *h*-BN was significantly higher compared to graphene, which was suggested to originate from the higher adsorption free energies of the amino acids.

Due to the success of C_2N in adsorbing and delivering nucleic acids, Zhou and co-workers evaluated the adsorption of HP35 on *h*2D-C_2N (Figure 10(g)).[118] It was revealed that the adsorption of HP35 on C_2N did not cause significant distortion to the secondary structure of the protein (Figure 10(h)). Additionally, the magnitudes of the protein-material interaction energies were less compared to those observed for the adsorption of prototypical proteins on graphene and *h*-BN. In contrast to graphene and *h*-BN, the adsorbed protein was highly restricted on the initial site of adsorption on C_2N, due to the presence of periodic potential wells present on the surface. It was concluded that the mild adsorption of the protein on C_2N was dominated by long-range electrostatic interactions rather than vdW interactions, and therefore, the constituent residues were able to interact with C_2N without disrupting their native arrangement. The same group studied the adsorption of the same protein on C_3N, another carbon nitride polyaniline 2D material.[119] In complete contrast to the behavior of C_2N, HP35 underwent partial denaturation, and the α-helical content of the protein was significantly reduced to random coils. The driving force was found to be predominat vdW interactions compared to electrostatics, a behavior opposite to that observed for the adsorption on C_2N, thereby causing the amino acid residues to disrupt their secondary structures. Therefore, C_2N was predicted to be biocompatible and non-nanotoxic toward protein, while C_3N demonstrates significant denaturating effects. The biocompatible property was not generalized for all nitrogen-doped graphene-based materials; rather, it was dependent on the subtle balance between electrostatics and vdW interactions.

Another 2D material, phosphorene, was subject to evaluation for its nanotoxicity toward proteins, by Zhang et al., employing a signal protein WW domain.[120] They observed two types of structural disruption of the protein native structure depending on the orientation of adsorption. In the first mechanism, the secondary structure of the protein remained intact; however, the ligand PRM was snatched from the protein followed by blocking of the active site. Alternatively, in the other mechanism, the β-sheet structure of the WW domain was completely disrupted, but the ligand position was intact. In both cases, the native function of the signal protein was lost. The debate regarding the nanotoxicity of some of the above materials was settled by Liu et al. by

https://doi.org/10.1021/acsphyschemau.3c00053
ACS Phys. Chem Au 2024, 4, 97−121

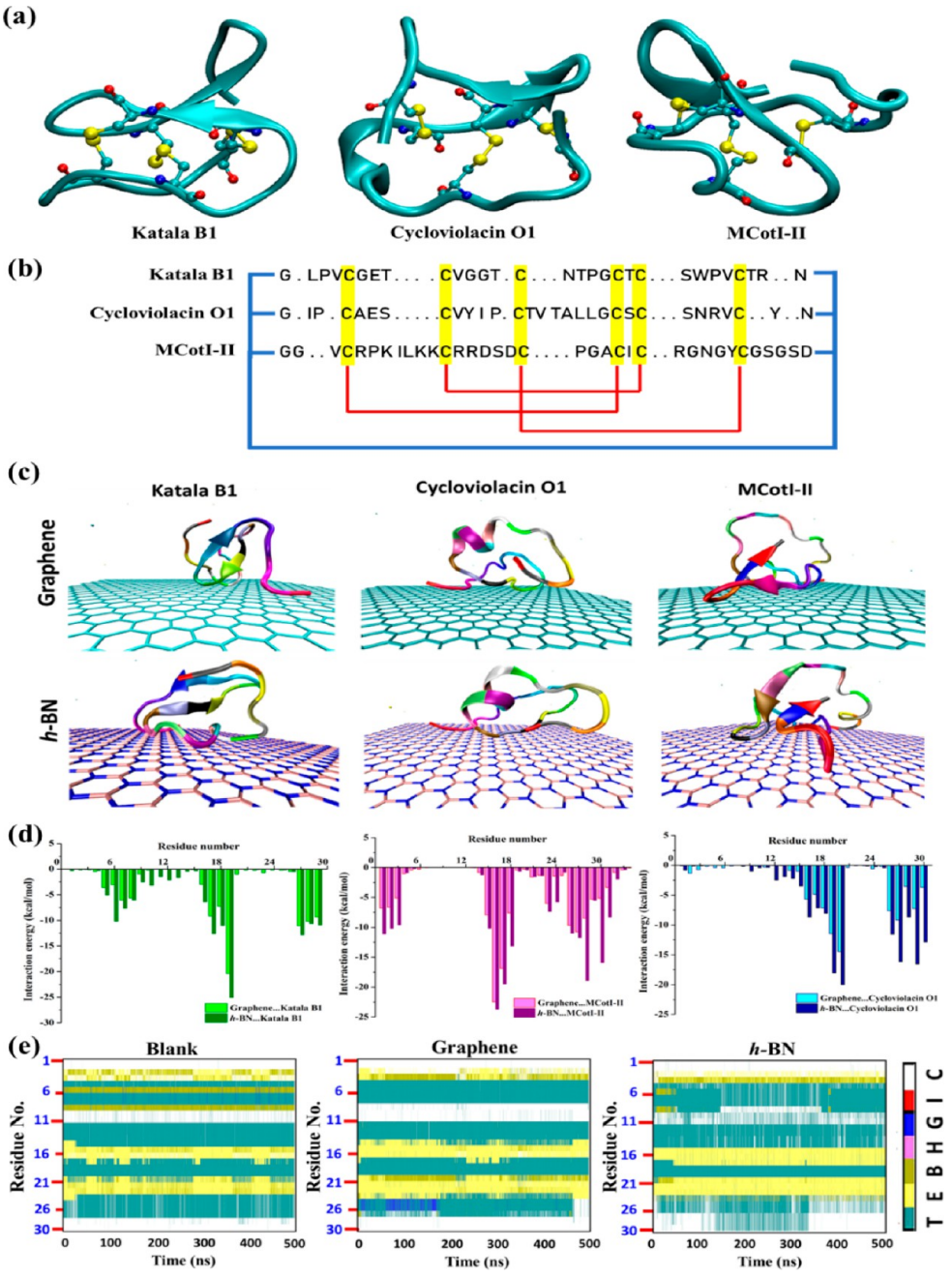

Figure 11. (a) Secondary structures of model cyclotides, namely, katala B1 (Möbius), cycloviolacin O1 (bracelet), and MCoTI-II (cyclic knottin). (b) Amino acids sequences of the cyclotides. Cystine residues are highlighted in yellow, the cyclic knots are represented by red lines, and the connections between residues are shown by blue lines. (c) Snapshots representing the adsorbed structure of cyclotides on graphene and h-BN. (d) Time evolution of the secondary structures of katala B1 in absence of any 2D material and during adsorption on graphene and h-BN. Reprinted with permission from ref 132, copyright 2022, the Royal Society of Chemistry.

studying the adsorption of several model proteins on graphene, phosphorene, and C_2N.[121] They found that graphene disrupted both the α-helical and β-sheet structures, the former being affected to a greater extent. On the other hand, the α-helical structure changed slightly on the BP surface, while the β-sheet maintained its structural integrity. For the adsorption of the proteins on C_2N, all of the secondary structures were preserved completely, thereby behaving as a nontoxic and biocompatible 2D material.

3.2. Biocompatibility of 2D Materials toward Cyclotides

The results discussed above clearly suggest that several 2D materials are nanotoxic to proteins, with graphene and *h*-BN being the most toxic, followed by other materials such as C_3N among others. However, proteins that are extremely resistant to typical denaturants could be adsorbed on nanotoxic 2D materials such as graphene and *h*-BN without structural disruption. Less nanotoxic 2D materials, such as C_2N, and C_3N_4 would certainly have little impact on their structures. Cyclotides, a family of topologically fascinating disulfide-rich plant peptides with 28 to 37 amino acid residues, is one of the well-known peptides with high stability.[122,123] The cyclotides

https://doi.org/10.1021/acsphyschemau.3c00053
ACS Phys. Chem Au 2024, 4, 97−121

Table 4. Free Energies (in kcal/mol) and Release Times for Single Cyclotide Molecules and Their Aggregates on 2D Materials: Average Adsorption Free Energy Per Cyclotide in an Aggregate ($\Delta G_{ad,agg}^{single}$), Free Energy of Adsorption for a Single Cyclotide (ΔG_{ad}^{single}), Free Energy Loss Per Molecule (ΔG_{loss}), Release Times for a Single Adsorbed Cyclotide ($r_{release}^{single}$), and Release Times for a Single Cyclotide from an Adsorbed Aggregate ($r_{release}^{agg}$)[a]

Cyclotide	2D Material	$\Delta G_{ad,agg}^{single} = \Delta G_{ad}^{agg}/4$	ΔG_{ad}^{single}	ΔG_{loss}	$r_{release}^{single}$ (ns)	$r_{release}^{agg}$ (ns)
Cycloviolacin O1	**Graphene**	−12.8	−30.4	17.6	1.30×10^{23}	1.46×10^{10}
	h-**BN**	−15.0	−34.2	19.2	1.63×10^{26}	2.60×10^{12}
Katala B1	**Graphene**	−11.8	−25.3	13.5	9.03×10^{19}	1.55×10^{10}
	h-**BN**	−13.8	−31.9	18.1	1.42×10^{24}	1.25×10^{11}
MCoTI-II	**Graphene**	−15.9	−34.1	18.2	2.99×10^{26}	2.32×10^{13}
	h-**BN**	−18.3	−43.2	24.9	2.27×10^{32}	2.65×10^{14}

[a]Reprinted with permission from ref 132, copyright 2022, the Royal Society of Chemistry.

share a head-to-tail cyclized peptide backbone and three interlocking disulfide bridges built from six conserved cystine residues. A cyclic cystine knot (CCK) motif (Figure 11(a)) is formed when one of the disulfide bonds penetrates via a macrocycle formed from the other two disulfide bonds, thereby providing a rigid framework and resulting in exceptional thermal stability and resistance to denaturants.[124,125] Cyclotides may be classified into two categories depending on the presence of a cisproline (Pro) residue. Cyclotides that contain this Pro residue are called Möbius cyclotides (Figure 11(a)) while those for which the Pro residue is absent are referred to as Bracelet cyclotides (Figure 11(a)). Recently, another class of the cyclotides, the cyclic knottins, has been found which is distinct from the Möbius and Bracelet families (Figure 11(a)).[126] Cyclotides have been found to show strong hemolytic, antifouling, anti-HIV, antibacterial, and antifungal activity through selective membrane penetration and disruption.[127−130] On the other hand, both graphene and *h*-BN have also been found to show antibacterial activity, penetrating cell membranes through their sharp edges and disrupting the structure.[40,58,62,131] Therefore, it may be envisaged that the bio-nanocomposites of these materials with cyclotides may retain the antifungal, antibacterial, and anticancer effects of individuals and may even show improved cooperative effectiveness.

To test these hypotheses, we studied the adsorption of three cyclotides belonging to different families (Figure 11(b)) viz. katala B1 (Mobius), cycloviolacin O1 (Bracelet), and MCotI-II (cyclic knottin) on both graphene and *h*-BN.[132] Contrary to the results observed for other peptides and proteins, we did not observe any significant structural disruption of the cyclotides, as observed from the final structures of the peptides on both materials (Figure 11(c)). Secondary structural analysis showed that neither the α-helical nor the β-sheet content was reduced following adsorption on the 2D materials, and the time evolution of the secondary structure had patterns similar to those observed for blank simulations (Figure 11(e)). The interaction energy trends for the cyclotides followed the order MCoTI-II > Cycloviolacin O1 > Katala B1, the difference being attributed to the amino acid sequences. Calculation of the residue-wise interaction energies (Figure 11(d)) with the materials revealed significant insights. As observed from Figure 11(d), the strongly interacting amino acid residues are mostly common for both 2D materials. The residues Tyr, Trp, Arg, and Asn had an average interaction energy equal or more than −15 kcal/mol while Cys, Ser, Leu, and Ile had an interaction between −10 and −15 kcal/mol, corroborating with the free energy calculations by Hughes et al.[116] Additionally, Cys residues had significantly low interaction energy with the 2D materials, and therefore, the disulfide linkages were relatively free to protect the structure. Interestingly, Cycloviolacin O1 has only two aromatic residues (Tyr4 and Tyr23), while both Katala B1 and MCoTI-II have only one aromatic residue (Trp19 and Tyr32). Even though the average interaction energies of the aromatic residues with both 2D materials were larger than −15 kcal/mol, their overall contribution to the total interaction energy was minimal. Therefore, the lesser abundance of aromatic residues in the cyclotide sequence contributes to the increased stability and conservation of the secondary structure.

Cyclotides exist in plants mostly in aggregated states, while they operate in both single and aggregated forms. Therefore, we studied the interaction between aggregated cyclotides and the 2D materials. It was observed that cyclotide aggregates could spontaneously adsorb on the materials without distorting their structures. Adsorption free energies were calculated for single cyclotide molecules (ΔG_{ad}^{single}) from an adsorbed state and from an adsorbed aggregate ($\Delta G_{ad,agg}^{single}$). The free energy profiles were inserted in eq 2, and the release times (Table 4) were calculated accordingly. The calculated release times for single molecules ($r_{release}^{single}$) follow the same trend as observed for the adsorption free energies on any of the 2D materials, i.e., Katala B1 < Cycloviolacin O1 < MCoTI-II, and the release time from *h*-BN is 10^3−10^6 times higher than that observed from graphene. However, magnitudes of $r_{release}^{single}$ clearly suggest that the adsorbed cyclotide molecules are not expected to be desorbed from the 2D materials during the interaction with chemical substances upon entering the physiological environment. Consequently, we could safely conclude that the adsorption of the cyclotides on 2D materials is mild, although it is sufficiently strong to form stable heterostructures. The situation of the aggregate was investigated indirectly, and the average free energy of adsorption of a single cyclotide ($\Delta G_{ad,agg}^{single}$) in the aggregates was obtained dividing the free energy of adsorption of the aggregate (ΔG_{ad}^{agg}) by the number of cyclotides. It was revealed that with addition of more and more cyclotides, the average adsorption free energy was reduced, which in turn also reduced the release time of the cyclotides from the adsorbed aggregates ($r_{release}^{agg}$) by orders of magnitude. It is conceivable that controlling the size of the aggregates may offer the opportunity to fine-tune the degree of interaction between 2D materials and cyclotides, which would increase the propensity for sustained release of individual peptides from the aggregates, thus giving an opportunity to interact with other biomolecules. Alternatively, the adsorption affinity of cyclotide can further be adjusted by introducing different functionalization into the 2D material or by controlling the degree of oxidation of the material.

https://doi.org/10.1021/acsphyschemau.3c00053
ACS Phys. Chem Au 2024, 4, 97−121

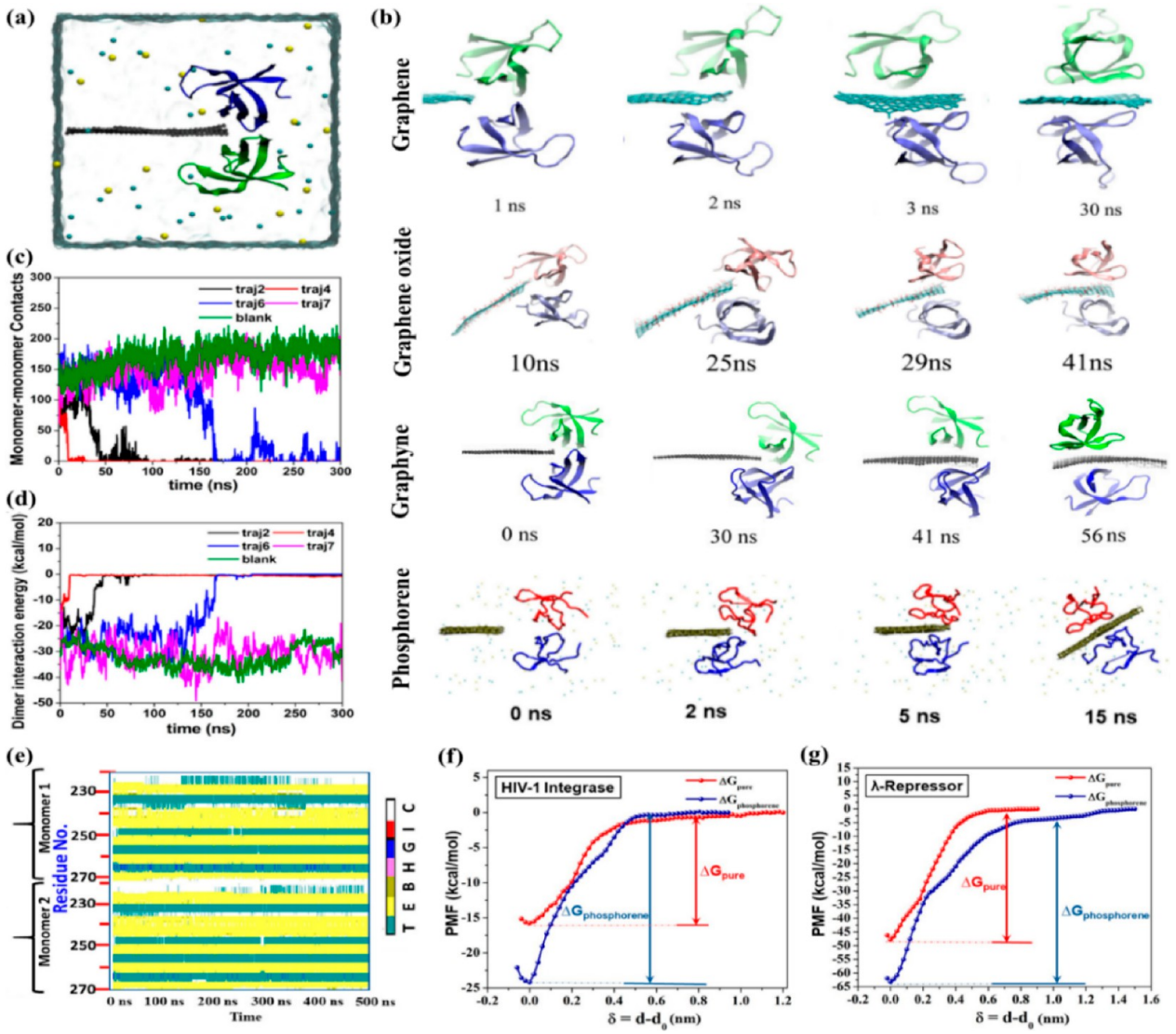

Figure 12. (a) Initial structure of the dimer cleavage simulations employing 2D materials; (b) representative snapshots for the interaction of 2D materials with a dimeric protein HIV-1 integrase. Time evolution of the intermonomer (c) contacts and (d) interaction energy for several successful (traj2, traj4, traj6) and one failed (traj8) trajectory for the cleavage simulations of HIV-1 integrase and phosphorene, and (e) secondary structure of HIV-1 integrase after being separated by phosphorene. Adsorption free energies of a protein monomer with another monomer in a dimeric structure (ΔG_{pure}) and a hydrogen-terminated phosphorene surface ($\Delta G_{phosphorene}$) for (f) HIV-1 integrase and (g) λ-repressor. Images have been reprinted with permission from ref 42, copyright 2014 American Chemical Society, ref 135, copyright 2016, AIP publishing, ref 136, copyright 2016 American Chemical Society, and ref 137, copyright 2021 American Chemical Society.

3.3. Cleavage of Dimeric Proteins Using 2D Materials

One of the significant methods of the functioning of proteins is protein−protein interactions (PPIs), and proteins are known to carry out several biological functions predominantly through PPIs, such as signal transduction, and cell metabolism.[133] In addition, there are a large number of multidomain proteins, which act in their assembled state, and therefore, loss in PPI can lead to the disruption of biological functions, resulting in several diseases.[134] Since it has already been established that proteins can strongly adsorb on 2D materials, it is obvious to inspect if they can disrupt PPIs and cleave multidomain protein structures.

Zhou and co-workers designed a computational protocol to decipher such interactions and applied the protocol for evaluating the interactions between a dimeric protein HIV-1 integrase and graphene, graphene oxide, and graphyne.[42,135,136] We applied a similar strategy to deduce the possidimeric protein cleavage probability of black phosphorene (BP), taking HIV-1 integrase and the λ_{6-85} repressor protein as the substrates.[137] HIV-1 integrase exists as a homodimer of two identical monomers, each containing a five-stranded antiparallel β-barrel and a three-residue 3_{10}-helix. In all the simulations, the 2D material was placed close to the dimeric interface (Figure 12(a)) and simulations were continued to observe whether the material enters the interface and separates both the monomers. It was found that all of the above-mentioned 2D materials were able to cleave the monomeric units of HIV-1 integrase, as observed in the representative snapshots in Figure 12(b)). The process of dimer cleavage could be characterized by a decrease in the contact surface area (Figure 12(c)) and the interaction energies (Figure 12(d)) between the two monomers. However, there was no definite time scale of these cleavages, the process being dependent on the spatial orientation of the material to the dimeric protein as

https://doi.org/10.1021/acsphyschemau.3c00053
ACS Phys. Chem Au 2024, 4, 97−121

well as the probability of the interaction of the material with the dimer interface. In the case of several trajectories simulated for the dimer cleavage simulations for any material, different trajectories usually yielded the dimer separation event at different time scales, and no one-to-one correlation existed for the observed time scales for different materials (Figure 12(b)). A careful inspection of the snapshots obtained from the concerned articles suggested that a perpendicular arrangement of the material with respect to the axis of the protein dimer allows the material to enter the interface leading to cleavage while a parallel arrangement induces sidewise interactions between the protein with the material, thereby resulting in regular adsorption without dimer cleavage. Time evolution of the intermonomer contact surface area and the interaction energy for such a failed trajectory (trajectory-7) is provided in Figure 12(c) and 12(d), where the magnitudes of these quantities were very similar to those observed in a blank simulation. Also, if the material became distant from the dimeric interface and abruptly changed its spatial orientation due to solvent-induced fluctuation and/or thermal effects, it could not take part in cleavage in computationally accessible time scales.[135,137] We also investigated the time evolution of the secondary structure of the HIV-1 integrase and the λ_{6-85} repressor proteins upon adsorption on BP to check whether the protein shows nanotoxicity through the alteration of the secondary structures.[137] The proteins were strategically chosen, since HIV-1 integrase predominantly consisted of a β sheet structure while λ_{6-85} repressor was mostly alpha helical. In both cases, we did not observe significant changes of the secondary structures (Figure 12(e)), thereby arriving at the suggestion that adsorption of proteins on BP had little to no perturbing effect on their structures. The cleavage of the dimers could be considered as a "clean-cut", and it was predicted that BP might be used as a "green" 2D material for cleaving polymeric structures of proteins without structural disruption. Therefore, most of the 2D materials show toxicity through the separation of the different monomeric domains of polymeric proteins and also disrupt their secondary structures. It might not be safe to administer these 2D materials into a cellular environment; however, BP, in particular, might be used in the fabrication of bionano devices intended for the cleavage of biomolecules and can act as a potent therapeutic agent against HIV.

Furthermore, a free energy calculation protocol was devised to investigate the thermodynamic basis for the nanomaterial insertion.[137] Two different adsorption free energies were determined, namely, the free energy of binding between the two protein monomers (ΔG_{pure}) and the adsorption free energy of a monomer on phosphorene ($\Delta G_{phosphorene}$). The thermodynamic preference for material insertion was estimated in terms of the free energy gain ($\Delta\Delta G_{pref}$) when two monomers dissociate and each of them get adsorbed on the surface of the phosphorene sheet, according to the relation $\Delta\Delta G_{pref} = 2\Delta G_{phosphorene} - \Delta G_{pure}$, and Figure 12(f) and 12(g) depicts the ΔG_{pure} and $\Delta G_{phosphorene}$ values for the two proteins. The calculated magnitudes of ΔG_{pref} were −32.1 and −78.6 kcal/mol for HIV-1 integrase and λ-repressor, respectively. Therefore, insertion of the phosphorene nanosheet was thermodynamically favorable for both of the protein dimers provided the 2D material had a preferable orientation to get inserted across the dimeric interface before approaching any other plausible mode of interaction. The thermodynamic preference was explained in terms of the significantly higher magnitude of the adsorption free energy between any of the protein monomers and phosphorene, which largely outweighed the intermonomer free energy of binding. The outlined free energy strategy can further be used in determining the possibility of cleavage of multidomain proteins employing any 2D material.

4. LIMITATIONS

Despite being able to predict the consequences of the interactions between 2D materials and biomolecules such as lipids, proteins, and nucleic acids, computational methods suffer from several limitations as well. One of the major drawbacks of classical MD simulations is the reliability of force-field parameters for 2D materials used to model such interactions.[138] Traditionally, MD force-field parameters had been generated for common biomolecules and small organic molecules, and they have undergone decades of refinement through careful recalibration, parametrization, and fine-tuning. Regrettably, the parameters for most of the 2D materials have only been developed recently, and even though these parameters are capable of predicting the major physical properties such as Young's and bulk modulus, water interactions and contact angles, interactions with nonaqueous solvent and liquid-phase exfoliation, the accuracy of these parameters in modeling physiological environments is largely unknown and requires substantiation through experimental verification of the computationally predicted outcomes. Nevertheless, in several instants, the computational results have been found to corroborate experimental expeditions.[37,139−141] In addition, the partial charges on the atoms that make up 2D materials have also been produced by using small molecular models of infinitely large material sheets. These partial charges depend on the level of theory employed and may not be consistent with those used for biomolecular species, which might result in an overestimation or underestimation of the interaction energies between them.[142] Therefore, to get close agreement between cytotoxicity experiments and computationally evaluated toxicity results, the force-field parameters must be fine-tuned through continuous calibration using experimental data. A decade earlier, such experimental results were a handful, and as a result, quality control of the MD parameters for 2D materials was problematic. Additionally, it has been an ongoing challenge for computational chemists and material scientists to provide these parameters on demand given the recent acceleration in the discovery of novel 2D materials. Fortunately, nowadays, with the remarkable advancement of nanotechnology, advanced experimental techniques are being used to produce high-quality data sets, which has made the validation of the MD parameters substantially easier, thereby pacing up the development of considerably accurate force-fields. For instance, the newly developed polarizable force-field parameters for nanomaterials have markedly enhanced the accuracy of the biomolecule-nanomaterial interactions, especially in those cases where the presence of the biomolecules affects the electronic distribution of the materials and vice versa. In addition, the bionano community has been hugely benefitted through the development of all-atoms force-field libraries such as CHARMM General Force Field (CGenFF) and General Amber Force Field (GAFF), since they provide common atom types related to several 2D materials.[99,143,144] It is expected that with the advancement in force-field development strategies and introduction of machine learning

https://doi.org/10.1021/acsphyschemau.3c00053
ACS Phys. Chem Au 2024, 4, 97−121

protocols, high-quality MD parameters for low-dimensional nanomaterials would be developed, thereby providing computational material scientists a huge boost for the screening of 2D materials for their toxic effects.

The other drawback that MD faces is the size-limitation of the simulation systems, which in turn directly affects the computationally accessible time scales for investigations. Biological systems are large enough to encompass an enormous variety of biomolecules; therefore, mimicking the biological environment inevitably demands large size of the simulation systems, the number of atoms varying between thousands to millions. However, the larger the system size, the smaller the accessible time scales of simulation. The events related to nanotoxicity occur on the time scale of hours to days, and hence, computer simulations of nanoseconds and even microseconds may not be adequate to produce the desired events. A good example would be refolding of 2D material-unfolded proteins, which is not expected to happen within the usual accessible computational time scales. While AIMD and reactive force-field simulations can be used to study the possibility of chemical reactions between 2D materials and biomolecules such as the generation of reactive-oxygen species (ROS), one of the common pathways of nanomaterial-induced toxicity in physiological environment, the accessibility of extremely low computational time scales of only hundreds of picoseconds for large biological systems has made these techniques futile in this context. Nonetheless, remarkable development of high-performance supercomputing technologies during the past decade has made it possible to simulate millions of atoms for a few hundreds of nanoseconds and is expected to achieve much longer time scales for both classical and AIMD in the near future, which in turn would be indispensable for the high-throughput computational screening of materials for biomedical purposes.

5. CONCLUSIONS AND OUTLOOK

In summary, this feature article outlines the methodologies adopted for the computational evaluation of the nanotoxicity of 2D nanomaterials toward nucleic acids and proteins, employing DFT and classical as well as ab initio MD techniques. The temporal development and continuous progress in computational protocols have been discussed, taking various 2D materials as platforms for biomolecular interactions. DFT and MD studies suggest that the possibility of the chemical reactions between 2D materials and biomolecules is less and interaction between these substances takes place via adsorption through noncovalent forces such as van der Waals interactions, hydrophobic association, and $\pi-\pi$ stacking along with long-range electrostatic interactions. From the careful inspection of the nature and mode of such interactions, it may be put forward that a subtle balance between the van der Waals and electrostatic interactions controls the outcome of the interaction event. The high strength and predominance of vdW interactions over the electrostatic interactions between 2D materials and biomolecules tend to destroy the internal spatial arrangement of various residues in biomolecules, leading to a significant disruption of secondary and tertiary structures, which in turn causes nanotoxicity. Graphene, *h*-BN, and C_3N display nanotoxicity via this mechanism. In another scenario, where both vdW and electrostatic interaction energies are significantly high, the structures of biomolecules are perturbed, and graphene oxide exhibits nanotoxicity in this fashion. On the other hand, when the electrostatic interactions are predominant along with weak vdW interactions, the biomolecules prefer to interact from a larger distance with the 2D materials without perturbing the internal native disposition, thereby behaving as a biocompatible material. *h*2D-C_2N and g-C_3N_4 belong to this category and are biocompatible toward genres of biomolecules. Indeed, both experimental and computational studies reveal that *h*2D-C_2N is one of the most biocompatible 2D materials found to date. In the last scenario, where both vdW and electrostatic interactions between the 2D materials and the biomolecules are weak, the adsorption is mild and does not affect the structure or function of the biomolecules. Several transition-metal dichalcogenides such as MoS_2 and $MoSe_2$ fall under this category. In addition, surface inhomogeneity, defects, and chemical modifications of 2D nanomaterials can modify the balance between the vdW and electrostatic interactions, thereby leading to the alteration of the nanotoxic effects. Accordingly, surface passivation and chemical functionalization may be utilized to reduce the nanotoxicity of these materials.

In general, evaluating the nanotoxicity of 2D materials is a complex task that can be accomplished by using both experimental and computational techniques. *In silico* methods have the advantage of identifying molecular interactions leading to nanotoxicity and, therefore, have the potential to complement *in vivo* and *in vitro* studies. To date, computational techniques, particularly MD simulations, have proven to be effective and efficient in predicting such properties. However, high-throughput screening of nanotoxicity would require a better design of simulation protocols and is very important for future research. The use of machine learning methods and force fields can accomplish this goal as long as the accuracy of the results is not compromised. Another question to be answered is the reconstruction of the secondary and tertiary structures of nucleic acids and proteins after their release from 2D materials. Targeted and accelerated MD simulations along with advanced sampling techniques such as replica-exchange MD might be used for this purpose, although it would use extensive computational resources. The potential for long-term cytotoxicity of 2D nanomaterials to host cells also requires further computational studies of dosage and exposure time. To conclude, although *in silico* approaches carry the potential to predict and screen 2D materials for their nanotoxicity, the exact physiological effects must be confirmed from experiments prior to their application in bio-nanomedicine. We strongly believe that the computational approaches discussed in this paper would inspire computational chemists, biologists, and material scientists to develop improved methods and simulation protocols for the *in silico* assessment of cytotoxicity, thereby paving the way for the applications of 2D materials to meet the existing and imminent demands for nontoxic bionano devices and therapeutics.

AUTHOR INFORMATION

Corresponding Author

Ayan Datta − *School of Chemical Sciences, Indian Association for the Cultivation of Science, Kolkata 700032 West Bengal, India;* orcid.org/0000-0001-6723-087X; Email: spad@iacs.res.in

Authors

Titas Kumar Mukhopadhyay − *School of Chemical Sciences, Indian Association for the Cultivation of Science, Kolkata*

https://doi.org/10.1021/acsphyschemau.3c00053
ACS Phys. Chem Au 2024, 4, 97−121

700032 West Bengal, India; orcid.org/0000-0003-2505-6732

Anupam Ghosh − *School of Chemical Sciences, Indian Association for the Cultivation of Science, Kolkata 700032 West Bengal, India*

Complete contact information is available at: https://pubs.acs.org/10.1021/acsphyschemau.3c00053

Author Contributions

CRediT: **Titas Kumar Mukhopadhyay** data curation, formal analysis, writing-original draft, writing-review & editing; **Anupam Ghosh** investigation, methodology, validation, visualization, writing-original draft, writing-review & editing; **Ayan Datta** conceptualization, funding acquisition, project administration, supervision.

Notes

The authors declare no competing financial interest.

■ ACKNOWLEDGMENTS

A.G. acknowledges CSIR for a Senior Research Fellowship (SRF). A.D. thanks SERB (grant CRG/2020/000301) for partial funding. We thank IACS for the use of TRC and CRAY supercomputers for computational purposes.

■ REFERENCES

(1) Novoselov, K. S.; Geim, A. K.; Morozov, S. V.; Jiang, D.; Zhang, Y.; Dubonos, S. V.; Grigorieva, I. V.; Firsov, A. A. Electric Field Effect in Atomically Thin Carbon Films. *Science* **2004**, *306*, 666−669.

(2) Novoselov, K. S.; Jiang, D.; Schedin, F.; Booth, T. J.; Khotkevich, V. V.; Morozov, S. V.; Geim, A. K. Two-dimensional atomic crystals. *Proc. Natl. Acad. Sci. U. S. A.* **2005**, *102*, 10451−10453.

(3) Chen, W.; Chen, S.; Qi, D. C.; Gao, X. Y.; Wee, A. T. S. Surface Transfer p-Type Doping of Epitaxial Graphene. *J. Am. Chem. Soc.* **2007**, *129*, 10418−10422.

(4) Meyer, J. C.; Geim, A. K.; Katsnelson, M. I.; Novoselov, K. S.; Obergfell, D.; Roth, S.; Girit, C.; Zettl, A. On the roughness of single- and bi-layer graphene membranes. *Solid State Commun.* **2007**, *143*, 101−109.

(5) Huo, C.; Yan, Z.; Song, X.; Zeng, H. 2D materials via liquid exfoliation: a review on fabrication and applications. *Sci. Bull.* **2015**, *60*, 1994−2008.

(6) Yang, J.; Yan, D.; Jones, T. S. Molecular Template Growth and Its Applications in Organic Electronics and Optoelectronics. *Chem. Rev.* **2015**, *115*, 5570−5603.

(7) Taylor-Pashow, K. M. L.; Della Rocca, J.; Huxford, R. C.; Lin, W. Hybrid nanomaterials for biomedical applications. *Chem. Commun.* **2010**, *46*, 5832−5849.

(8) Bitounis, D.; Ali-Boucetta, H.; Hong, B. H.; Min, D.-H.; Kostarelos, K. Prospects and Challenges of Graphene in Biomedical Applications. *Adv. Mater.* **2013**, *25*, 2258−2268.

(9) Chung, C.; Kim, Y.-K.; Shin, D.; Ryoo, S.-R.; Hong, B. H.; Min, D.-H. Biomedical Applications of Graphene and Graphene Oxide. *Acc. Chem. Res.* **2013**, *46*, 2211−2224.

(10) Chimene, D.; Alge, D. L.; Gaharwar, A. K. Two-Dimensional Nanomaterials for Biomedical Applications: Emerging Trends and Future Prospects. *Adv. Mater.* **2015**, *27*, 7261−7284.

(11) Xu, W.; Mao, N.; Zhang, J. Graphene: A Platform for Surface-Enhanced Raman Spectroscopy. *Small* **2013**, *9*, 1206−1224.

(12) Valeš, V.; Drogowska-Horná, K.; Guerra, V. L. P.; Kalbáč, M. Graphene-enhanced Raman scattering on single layer and bilayers of pristine and hydrogenated graphene. *Sci. Rep.* **2020**, *10*, 4516.

(13) Sun, X.; Liu, Z.; Welsher, K.; Robinson, J. T.; Goodwin, A.; Zaric, S.; Dai, H. Nano-graphene oxide for cellular imaging and drug delivery. *Nano Res.* **2008**, *1*, 203−212.

(14) Zhang, L.; Xia, J.; Zhao, Q.; Liu, L.; Zhang, Z. Functional Graphene Oxide as a Nanocarrier for Controlled Loading and Targeted Delivery of Mixed Anticancer Drugs. *Small* **2010**, *6*, 537−544.

(15) Feng, L.; Zhang, S.; Liu, Z. Graphene based gene transfection. *Nanoscale* **2011**, *3*, 1252−1257.

(16) Chen, B.; Liu, M.; Zhang, L.; Huang, J.; Yao, J.; Zhang, Z. Polyethylenimine-functionalized graphene oxide as an efficient gene delivery vector. *J. Mater. Chem.* **2011**, *21*, 7736−7741.

(17) Liu, K.; Zhang, J.-J.; Cheng, F.-F.; Zheng, T.-T.; Wang, C.; Zhu, J.-J. Green and facile synthesis of highly biocompatible graphene nanosheets and its application for cellular imaging and drug delivery. *J. Mater. Chem.* **2011**, *21*, 12034−12040.

(18) Peng, C.; Hu, W.; Zhou, Y.; Fan, C.; Huang, Q. Intracellular Imaging with a Graphene-Based Fluorescent Probe. *Small* **2010**, *6*, 1686−1692.

(19) Li, N.; Zhang, X.; Song, Q.; Su, R.; Zhang, Q.; Kong, T.; Liu, L.; Jin, G.; Tang, M.; Cheng, G. The promotion of neurite sprouting and outgrowth of mouse hippocampal cells in culture by graphene substrates. *Biomater.* **2011**, *32*, 9374−9382.

(20) Kalbacova, M.; Broz, A.; Kong, J.; Kalbac, M. Graphene substrates promote adherence of human osteoblasts and mesenchymal stromal cells. *Carbon* **2010**, *48*, 4323−4329.

(21) Barati Farimani, A.; Dibaeinia, P.; Aluru, N. R. DNA Origami-Graphene Hybrid Nanopore for DNA Detection. *ACS Appl. Mater. Interfaces* **2017**, *9*, 92−100.

(22) Barati Farimani, A.; Heiranian, M.; Min, K.; Aluru, N. R. Antibody Subclass Detection Using Graphene Nanopores. *J. Phys. Chem. Lett.* **2017**, *8*, 1670−1676.

(23) Chen, Y.; Tan, C.; Zhang, H.; Wang, L. Two-dimensional graphene analogues for biomedical applications. *Chem. Soc. Rev.* **2015**, *44*, 2681−2701.

(24) Kurapati, R.; Kostarelos, K.; Prato, M.; Bianco, A. Biomedical Uses for 2D Materials Beyond Graphene: Current Advances and Challenges Ahead. *Adv. Mater.* **2016**, *28*, 6052−6074.

(25) Lee, H. U.; Park, S. Y.; Lee, S. C.; Choi, S.; Seo, S.; Kim, H.; Won, J.; Choi, K.; Kang, K. S.; Park, H. G.; Kim, H.-S.; An, H. R.; Jeong, K.-H.; Lee, Y.-C.; Lee, J. Black Phosphorus (BP) Nanodots for Potential Biomedical Applications. *Small* **2016**, *12*, 214−219.

(26) Luo, M.; Fan, T.; Zhou, Y.; Zhang, H.; Mei, L. 2D Black Phosphorus-Based Biomedical Applications. *Adv. Funct. Mater.* **2019**, *29*, 1808306.

(27) Peng, J.; Wang, S.; Zhang, P.; Jiang, L.; Shi, J.; Zhu, J. J. Fabrication of graphene quantum dots and hexagonal boron nitride nanocomposites for fluorescent cell imaging. *J. Biomed. Nanotechnol.* **2013**, *9*, 1679−85.

(28) Fiume, M. M.; Bergfeld, W. F.; Belsito, D. V.; Hill, R. A.; Klaassen, C. D.; Liebler, D. C.; Marks, J. G.; Shank, R. C.; Slaga, T. J.; Snyder, P. W.; Andersen, F. A. Safety Assessment of Boron Nitride as Used in Cosmetics. *Int. J. Toxicol.* **2015**, *34*, 53S−60S.

(29) Fojtů, M.; Chia, X.; Sofer, Z.; Masařík, M.; Pumera, M. Black Phosphorus Nanoparticles Potentiate the Anticancer Effect of Oxaliplatin in Ovarian Cancer Cell Line. *Adv. Funct. Mater.* **2017**, *27*, 1701955.

(30) Liu, Z.; Chen, H.; Jia, Y.; Zhang, W.; Zhao, H.; Fan, W.; Zhang, W.; Zhong, H.; Ni, Y.; Guo, Z. A two-dimensional fingerprint nanoprobe based on black phosphorus for bio-SERS analysis and chemo-photothermal therapy. *Nanoscale* **2018**, *10*, 18795−18804.

(31) Qiu, M.; Ren, W. X.; Jeong, T.; Won, M.; Park, G. Y.; Sang, D. K.; Liu, L.-P.; Zhang, H.; Kim, J. S. Omnipotent phosphorene: a next-generation, two-dimensional nanoplatform for multidisciplinary biomedical applications. *Chem. Soc. Rev.* **2018**, *47*, 5588−5601.

(32) Liu, K.; Feng, J.; Kis, A.; Radenovic, A. Atomically Thin Molybdenum Disulfide Nanopores with High Sensitivity for DNA Translocation. *ACS Nano* **2014**, *8*, 2504−2511.

(33) Ou, J. Z.; Chrimes, A. F.; Wang, Y.; Tang, S.-y.; Strano, M. S.; Kalantar-zadeh, K. Ion-Driven Photoluminescence Modulation of Quasi-Two-Dimensional MoS2 Nanoflakes for Applications in Biological Systems. *Nano Lett.* **2014**, *14*, 857−863.

(34) Lin, T.; Zhong, L.; Song, Z.; Guo, L.; Wu, H.; Guo, Q.; Chen, Y.; Fu, F.; Chen, G. Visual detection of blood glucose based on peroxidase-like activity of WS2 nanosheets. *Biosens. Bioelectron.* **2014**, *62*, 302−307.
(35) Rajh, T.; Dimitrijevic, N. M.; Bissonnette, M.; Koritarov, T.; Konda, V. Titanium Dioxide in the Service of the Biomedical Revolution. *Chem. Rev.* **2014**, *114*, 10177−10216.
(36) Elvira, G.; Moreno, B.; Valle, I. d.; Garcia-Sanz, J. A.; Canillas, M.; Chinarro, E.; Jurado, J. R.; Silva, A. Targeting Neural Stem Cells with Titanium Dioxide Nanoparticles Coupled to Specific Monoclonal Antibodies. *J. Biomater. Appl.* **2012**, *26*, 1069−1089.
(37) Liu, L.; Zhang, S.; Zhao, L.; Gu, Z.; Duan, G.; Zhou, B.; Yang, Z.; Zhou, R. Superior Compatibility of C2N with Human Red Blood Cell Membranes and the Underlying Mechanism. *Small* **2018**, *14*, 1803509.
(38) Lim, C. T.; Kenry, K. Biocompatibility and Nanotoxicity of Layered Two-Dimensional Nanomaterials. *ChemNanoMat* **2017**, *3*, 5.
(39) Wang, Z.; Zhu, W.; Qiu, Y.; Yi, X.; von dem Bussche, A.; Kane, A.; Gao, H.; Koski, K.; Hurt, R. Biological and environmental interactions of emerging two-dimensional nanomaterials. *Chem. Soc. Rev.* **2016**, *45*, 1750−1780.
(40) Hu, W.; Peng, C.; Luo, W.; Lv, M.; Li, X.; Li, D.; Huang, Q.; Fan, C. Graphene-Based Antibacterial Paper. *ACS Nano* **2010**, *4*, 4317−4323.
(41) Liao, K.-H.; Lin, Y.-S.; Macosko, C. W.; Haynes, C. L. Cytotoxicity of Graphene Oxide and Graphene in Human Erythrocytes and Skin Fibroblasts. *ACS Appl. Mater. Interfaces* **2011**, *3*, 2607−2615.
(42) Luan, B.; Huynh, T.; Zhao, L.; Zhou, R. Potential Toxicity of Graphene to Cell Functions via Disrupting Protein-Protein Interactions. *ACS Nano* **2015**, *9*, 663−669.
(43) Ciofani, G.; Danti, S.; Nitti, S.; Mazzolai, B.; Mattoli, V.; Giorgi, M. Biocompatibility of boron nitride nanotubes: An up-date of in vivo toxicological investigation. *Int. J. Pharm.* **2013**, *444*, 85−88.
(44) Augustine, J.; Cheung, T.; Gies, V.; Boughton, J.; Chen, M.; Jakubek, Z. J.; Walker, S.; Martinez-Rubi, Y.; Simard, B.; Zou, S. Assessing size-dependent cytotoxicity of boron nitride nanotubes using a novel cardiomyocyte AFM assay. *Nanoscale Adv.* **2019**, *1*, 1914−1923.
(45) Horváth, L.; Magrez, A.; Golberg, D.; Zhi, C.; Bando, Y.; Smajda, R.; Horváth, E.; Forró, L.; Schwaller, B. In Vitro Investigation of the Cellular Toxicity of Boron Nitride Nanotubes. *ACS Nano* **2011**, *5*, 3800−3810.
(46) Latiff, N. M.; Teo, W. Z.; Sofer, Z.; Fisher, A. C.; Pumera, M. The Cytotoxicity of Layered Black Phosphorus. *Chem.-Eur. J.* **2015**, *21*, 13991−13995.
(47) Song, S.-J.; Raja, I. S.; Lee, Y. B.; Kang, M. S.; Seo, H. J.; Lee, H. U.; Han, D.-W. Comparison of cytotoxicity of black phosphorus nanosheets in different types of fibroblasts. *Biomater. Res.* **2019**, *23*, 23−23.
(48) Yin, W.; Yan, L.; Yu, J.; Tian, G.; Zhou, L.; Zheng, X.; Zhang, X.; Yong, Y.; Li, J.; Gu, Z.; Zhao, Y. High-Throughput Synthesis of Single-Layer MoS2 Nanosheets as a Near-Infrared Photothermal-Triggered Drug Delivery for Effective Cancer Therapy. *ACS Nano* **2014**, *8*, 6922−6933.
(49) Yong, Y.; Zhou, L.; Gu, Z.; Yan, L.; Tian, G.; Zheng, X.; Liu, X.; Zhang, X.; Shi, J.; Cong, W.; Yin, W.; Zhao, Y. WS2 nanosheet as a new photosensitizer carrier for combined photodynamic and photothermal therapy of cancer cells. *Nanoscale* **2014**, *6*, 10394−10403.
(50) Cheng, L.; Liu, J.; Gu, X.; Gong, H.; Shi, X.; Liu, T.; Wang, C.; Wang, X.; Liu, G.; Xing, H.; Bu, W.; Sun, B.; Liu, Z. PEGylated WS2 Nanosheets as a Multifunctional Theranostic Agent for in vivo Dual-Modal CT/Photoacoustic Imaging Guided Photothermal Therapy. *Adv. Mater.* **2014**, *26*, 1886−1893.
(51) Teo, W. Z.; Chng, E. L. K.; Sofer, Z.; Pumera, M. Cytotoxicity of Exfoliated Transition-Metal Dichalcogenides (MoS2, WS2, and WSe2) is Lower Than That of Graphene and its Analogues. *Chem.-Eur. J.* **2014**, *20*, 9627−9632.
(52) Watson, J. D.; Crick, F. H. C. Molecular Structure of Nucleic Acids: A Structure for Deoxyribose Nucleic Acid. *Nature* **1953**, *171*, 737−738.
(53) Yakovchuk, P.; Protozanova, E.; Frank-Kamenetskii, M. D. Base-stacking and base-pairing contributions into thermal stability of the DNA double helix. *Nucleic Acids Res.* **2006**, *34*, 564−574.
(54) Zeng, S.; Chen, L.; Wang, Y.; Chen, J. Exploration on the mechanism of DNA adsorption on graphene and graphene oxide via molecular simulations. *J. Phys. D: Appl. Phys.* **2015**, *48*, 275402.
(55) Chen, J.; Chen, L.; Wang, Y.; Chen, S. Molecular dynamics simulations of the adsorption of DNA segments onto graphene oxide. *J. Phys. D: Appl. Phys.* **2014**, *47*, 505401.
(56) Xu, Z.; Lei, X.; Tu, Y.; Tan, Z.-J.; Song, B.; Fang, H. Dynamic Cooperation of Hydrogen Binding and π Stacking in ssDNA Adsorption on Graphene Oxide. *Chem.-Eur. J.* **2017**, *23*, 13100−13104.
(57) Ranganathan, S. V.; Halvorsen, K.; Myers, C. A.; Robertson, N. M.; Yigit, M. V.; Chen, A. A. Complex Thermodynamic Behavior of Single-Stranded Nucleic Acid Adsorption to Graphene Surfaces. *Langmuir* **2016**, *32*, 6028−6034.
(58) Mukhopadhyay, T. K.; Datta, A. Screening two dimensional materials for the transportation and delivery of diverse genetic materials. *Nanoscale* **2020**, *12*, 703−719.
(59) Gowtham, S.; Scheicher, R. H.; Ahuja, R.; Pandey, R.; Karna, S. P. Physisorption of nucleobases on graphene: Density-functional calculations. *Phys. Rev. B* **2007**, *76*, 033401.
(60) Le, D.; Kara, A.; Schröder, E.; Hyldgaard, P.; Rahman, T. Physisorption of nucleobases on graphene: A comparative van der Waals study. *J. Phys.: Condens. Matter* **2012**, *24*, 424210.
(61) Lee, J.-H.; Choi, Y.-K.; Kim, H.-J.; Scheicher, R. H.; Cho, J.-H. Physisorption of DNA Nucleobases on h-BN and Graphene: vdW-Corrected DFT Calculations. *J. Phys. Chem. C* **2013**, *117*, 13435−13441.
(62) Mukhopadhyay, T. K.; Bhattacharyya, K.; Datta, A. Gauging the Nanotoxicity of h2D-C2N toward Single-Stranded DNA: An in Silico Molecular Simulation Approach. *ACS Appl. Mater. Interfaces* **2018**, *10*, 13805−13818.
(63) Ghosh, S.; Dixit, H.; Chakrabarti, R. Ion assisted structural collapse of a single stranded DNA: A molecular dynamics approach. *Chem. Phys.* **2015**, *459*, 137−147.
(64) Mukhopadhyay, T. K.; Datta, A. Delicate Balance of Non-Covalent Forces Govern the Biocompatibility of Graphitic Carbon Nitride towards Genetic Materials. *ChemPhysChem* **2020**, *21*, 1836−1846.
(65) Johnson, R. R.; Johnson, A. T. C.; Klein, M. L. Probing the Structure of DNA-Carbon Nanotube Hybrids with Molecular Dynamics. *Nano Lett.* **2008**, *8*, 69−75.
(66) Zhao; Johnson, J. K. Simulation of Adsorption of DNA on Carbon Nanotubes. *J. Am. Chem. Soc.* **2007**, *129*, 10438−10445.
(67) Zou, J.; Liang, W.; Zhang, S. Coarse-grained molecular dynamics modeling of DNA-carbon nanotube complexes. *Int. J. Numer. Methods. Eng.* **2010**, *83*, 968−985.
(68) Johnson, R. R.; Kohlmeyer, A.; Johnson, A. T. C.; Klein, M. L. Free Energy Landscape of a DNA-Carbon Nanotube Hybrid Using Replica Exchange Molecular Dynamics. *Nano Lett.* **2009**, *9*, 537−541.
(69) Hughes, Z. E.; Walsh, T. R. Structural Disruption of an Adenosine-Binding DNA Aptamer on Graphene: Implications for Aptasensor Design. *ACS Sensors* **2017**, *2*, 1602−1611.
(70) Gu, Z.; Zhao, L.; Liu, S.; Duan, G.; Perez-Aguilar, J. M.; Luo, J.; Li, W.; Zhou, R. Orientational Binding of DNA Guided by the C2N Template. *ACS Nano* **2017**, *11*, 3198−3206.
(71) Malyshev, D. A.; Dhami, K.; Lavergne, T.; Chen, T.; Dai, N.; Foster, J. M.; Corrêa, I. R.; Romesberg, F. E. A semi-synthetic organism with an expanded genetic alphabet. *Nature* **2014**, *509*, 385−388.
(72) Mahmood, J.; Lee, E. K.; Jung, M.; Shin, D.; Choi, H.-J.; Seo, J.-M.; Jung, S.-M.; Kim, D.; Li, F.; Lah, M. S.; Park, N.; Shin, H.-J.; Oh, J. H.; Baek, J.-B. Two-dimensional polyaniline (C3N) from

https://doi.org/10.1021/acsphyschemau.3c00053
ACS Phys. Chem Au 2024, 4, 97−121

carbonized organic single crystals in solid state. *Proc. Natl. Acad. Sci. U. S. A.* **2016**, *113*, 7414−7419.
(73) Rani, S.; Ray, S. J. Two-dimensional C3N based sub-10 nm biosensor. *Phys. Chem. Chem. Phys.* **2020**, *22*, 11452−11459.
(74) Zhao, L.; Gu, Z. Potential Unwinding of Double-Stranded DNA upon Binding to a Carbon Nitride Polyaniline (C3N) Nanosheet. *J. Phys. Chem. B* **2021**, *125*, 2258−2265.
(75) Liu, F.; Zhang, Y.; Wang, H.; Li, L.; Zhao, W.; Shen, J.-W.; Liang, L. Study on the adsorption orientation of DNA on two-dimensional MoS2 surface via molecular dynamics simulation: A vertical orientation phenomenon. *Chem. Phys.* **2020**, *529*, 110546.
(76) Zhou, H.; Xie, Z.-X.; Liang, L.; Zhang, P.; Ma, X.; Kong, Z.; Shen, J.-W.; Hu, W. Theoretical investigation on the adsorption orientation of DNA on two-dimensional MoSe2. *Chem. Phys.* **2021**, *551*, 111329.
(77) Li, B.; Xie, X.; Duan, G.; Chen, S. H.; Meng, X.-Y.; Zhou, R. Binding patterns and dynamics of double-stranded DNA on the phosphorene surface. *Nanoscale* **2020**, *12*, 9430−9439.
(78) Kim, K. S.; Zhao, Y.; Jang, H.; Lee, S. Y.; Kim, J. M.; Kim, K. S.; Ahn, J.-H.; Kim, P.; Choi, J.-Y.; Hong, B. H. Large-scale pattern growth of graphene films for stretchable transparent electrodes. *Nature* **2009**, *457*, 706−710.
(79) Li, X.; Cai, W.; An, J.; Kim, S.; Nah, J.; Yang, D.; Piner, R.; Velamakanni, A.; Jung, I.; Tutuc, E.; Banerjee, S. K.; Colombo, L.; Ruoff, R. S. Large-Area Synthesis of High-Quality and Uniform Graphene Films on Copper Foils. *Science* **2009**, *324*, 1312−1314.
(80) Li, B.; Zhang, Y.; Meng, X.-Y.; Zhou, R. Zipper-Like Unfolding of dsDNA Caused by Graphene Wrinkles. *J. Phys. Chem. C* **2020**, *124*, 3332−3340.
(81) Gao, D.; Li, B.; Yang, Y.; Qu, Y.; Li, Y.-Q.; Zhao, M.; Liu, Y.; Liu, X.; Li, W. Defect-Induced Double-Stranded DNA Unwinding on Graphene. *J. Phys. Chem. B* **2021**, *125*, 2833−2840.
(82) Smirnov, I. V.; Shafer, R. H. Electrostatics dominate quadruplex stability. *Biopolymers* **2007**, *85*, 91−101.
(83) Luu, K. N.; Phan, A. T.; Kuryavyi, V.; Lacroix, L.; Patel, D. J. Structure of the Human Telomere in K+ Solution: An Intramolecular (3 + 1) G-Quadruplex Scaffold. *J. Am. Chem. Soc.* **2006**, *128*, 9963−9970.
(84) Špačková, N. a.; Berger, I.; Šponer, J. Nanosecond Molecular Dynamics Simulations of Parallel and Antiparallel Guanine Quadruplex DNA Molecules. *J. Am. Chem. Soc.* **1999**, *121*, 5519−5534.
(85) Evers, M. M.; Toonen, L. J. A.; van Roon-Mom, W. M. C. Antisense oligonucleotides in therapy for neurodegenerative disorders. *Adv. Drug Delivery Rev.* **2015**, *87*, 90−103.
(86) Paul, C. P.; Good, P. D.; Winer, I.; Engelke, D. R. Effective expression of small interfering RNA in human cells. *Nat. Biotechnol.* **2002**, *20*, 505−508.
(87) Morris, K. V.; Chan, S. W.-L.; Jacobsen, S. E.; Looney, D. J. Small Interfering RNA-Induced Transcriptional Gene Silencing in Human Cells. *Science* **2004**, *305*, 1289−1292.
(88) Lu, C.-H.; Zhu, C.-L.; Li, J.; Liu, J.-J.; Chen, X.; Yang, H.-H. Using graphene to protect DNA from cleavage during cellular delivery. *Chem. Commun.* **2010**, *46*, 3116−3118.
(89) Ke, P. C.; Qiao, R. Carbon nanomaterials in biological systems. *J. Phys.: Condens. Matter* **2007**, *19*, 373101.
(90) Ghosh, S.; Chakrabarti, R. Unzipping of Double-Stranded Ribonucleic Acids by Graphene and Single-Walled Carbon Nanotube: Helix Geometry versus Surface Curvature. *J. Phys. Chem. C* **2016**, *120*, 22681−22693.
(91) Maiti, M.; Maiti, M.; Knies, C.; Dumbre, S.; Lescrinier, E.; Rosemeyer, H.; Ceulemans, A.; Herdewijn, P. Xylonucleic acid: synthesis, structure, and orthogonal pairing properties. *Nucleic Acids Res.* **2015**, *43*, 7189−7200.
(92) Habibzadeh Mashatooki, M.; Sardroodi, J. J.; Ebrahimzadeh, A. R. Molecular Dynamics Investigation of the Interactions Between RNA Aptamer and Graphene-Monoxide/Boron-Nitride Surfaces: Applications to Novel Drug Delivery Systems. *J. Inorg. Organomet. Polym. Mater.* **2019**, *29*, 1252−1264.
(93) Perdew, J. P.; Zunger, A. Self-interaction correction to density-functional approximations for many-electron systems. *Phys. Rev. B* **1981**, *23*, 5048−5079.
(94) Møller, C.; Plesset, M. S. Note on an Approximation Treatment for Many-Electron Systems. *Phys. Rev.* **1934**, *46*, 618−622.
(95) Krishnan, R.; Binkley, J. S.; Seeger, R.; Pople, J. A. Self-consistent molecular orbital methods. XX. A basis set for correlated wave functions. *J. Chem. Phys.* **1980**, *72*, 650−654.
(96) Varghese, N.; Mogera, U.; Govindaraj, A.; Das, A.; Maiti, P. K.; Sood, A. K.; Rao, C. N. R. Binding of DNA Nucleobases and Nucleosides with Graphene. *ChemPhysChem* **2009**, *10*, 206−210.
(97) Sowerby, S. J.; Cohn, C. A.; Heckl, W. M.; Holm, N. G. Differential adsorption of nucleic acid bases: Relevance to the origin of life. *Proc. Natl. Acad. Sci. U. S. A.* **2001**, *98*, 820−822.
(98) Johnson, R. R.; Johnson, A. T. C.; Klein, M. L. The Nature of DNA-Base-Carbon-Nanotube Interactions. *Small* **2010**, *6*, 31−34.
(99) Vanommeslaeghe, K.; Hatcher, E.; Acharya, C.; Kundu, S.; Zhong, S.; Shim, J.; Darian, E.; Guvench, O.; Lopes, P.; Vorobyov, I.; Mackerell, A. D., Jr CHARMM general force field: A force field for drug-like molecules compatible with the CHARMM all-atom additive biological force fields. *J. Comput. Chem.* **2010**, *31*, 671−690.
(100) Sadeghi, M.; Jahanshahi, M.; Ghorbanzadeh, M.; Najafpour, G. Adsorption of DNA/RNA nucleobases onto single-layer MoS2 and Li-Doped MoS2: A dispersion-corrected DFT study. *Appl. Surf. Sci.* **2018**, *434*, 176−187.
(101) Mukhopadhyay, T.; Datta, A. Design Rules for the Generation of Stable Quartet Phases of Nucleobases over 2D Materials. *J. Phys. Chem. C* **2018**, *122*, 28918−28933.
(102) Patodia, S.; Bagaria, A.; Chopra, D. Molecular dynamics simulation of proteins: A brief overview. *J. Phys. Chem. Biophys.* **2014**, *4*, 1−4.
(103) Karplus, M.; McCammon, J. A. Molecular dynamics simulations of biomolecules. *Nat. Struct. Mol. Biol.* **2002**, *9*, 646−652.
(104) Guvench, O.; MacKerell, A. D. Comparison of Protein Force Fields for Molecular Dynamics Simulations. In *Molecular Modeling of Proteins;* Kukol, A., Ed.; Humana Press: Totowa, NJ, 2008; pp 63−88.
(105) Klepeis, J. L.; Lindorff-Larsen, K.; Dror, R. O.; Shaw, D. E. Long-timescale molecular dynamics simulations of protein structure and function. *Curr. Opin. Struct. Biol.* **2009**, *19*, 120−127.
(106) MacKerell, A. D.; Nilsson, L. Molecular dynamics simulations of nucleic acid-protein complexes. *Curr. Opin. Struct. Biol.* **2008**, *18*, 194−199.
(107) Piana, S.; Klepeis, J. L.; Shaw, D. E. Assessing the accuracy of physical models used in protein-folding simulations: quantitative evidence from long molecular dynamics simulations. *Curr. Opin. Struct. Biol.* **2014**, *24*, 98−105.
(108) Bernardi, R. C.; Melo, M. C. R.; Schulten, K. Enhanced sampling techniques in molecular dynamics simulations of biological systems. *Biochim. Biophys. Acta - Gen. Subj.* **2015**, *1850*, 872−877.
(109) Penna, M. J.; Mijajlovic, M.; Biggs, M. J. Molecular-Level Understanding of Protein Adsorption at the Interface between Water and a Strongly Interacting Uncharged Solid Surface. *J. Am. Chem. Soc.* **2014**, *136*, 5323−5331.
(110) Penna, M. J.; Mijajlovic, M.; Tamerler, C.; Biggs, M. J. Molecular-level understanding of the adsorption mechanism of a graphite-binding peptide at the water/graphite interface. *Soft Matter* **2015**, *11*, 5192−5203.
(111) Yu, J.; Becker, M. L.; Carri, G. A. The Influence of Amino Acid Sequence and Functionality on the Binding Process of Peptides onto Gold Surfaces. *Langmuir* **2012**, *28*, 1408−1417.
(112) Chen, S. H.; Bell, D. R.; Luan, B. Understanding interactions between biomolecules and two-dimensional nanomaterials using in silico microscopes. *Adv. Drug Delivery Rev.* **2022**, *186*, 114336.
(113) Guo, J.; Yao, X.; Ning, L.; Wang, Q.; Liu, H. The adsorption mechanism and induced conformational changes of three typical proteins with different secondary structural features on graphene. *RSC Adv.* **2014**, *4*, 9953−9962.
(114) Zuo, G.; Zhou, X.; Huang, Q.; Fang, H.; Zhou, R. Adsorption of Villin Headpiece onto Graphene, Carbon Nanotube, and C60:

https://doi.org/10.1021/acsphyschemau.3c00053
ACS Phys. Chem Au 2024, 4, 97−121

Effect of Contacting Surface Curvatures on Binding Affinity. *J. Phys. Chem. C* **2011**, *115*, 23323−23328.
(115) Wei, S.; Zou, X.; Tian, J.; Huang, H.; Guo, W.; Chen, Z. Control of Protein Conformation and Orientation on Graphene. *J. Am. Chem. Soc.* **2019**, *141*, 20335−20343.
(116) Hughes, Z. E.; Walsh, T. R. What makes a good graphene-binding peptide? Adsorption of amino acids and peptides at aqueous graphene interfaces. *J. Mater. Chem. B* **2015**, *3*, 3211−3221.
(117) Paul, S.; Mukhopadhyay, T. K.; Paul, S. In Silico Investigation on the Selective Nanotoxicity of Two-Dimensional Materials to Hen Egg White Lysozyme Protein. *ACS Appl. Nano Mater.* **2023**, *6*, 6504−6517.
(118) Li, B.; Li, W.; Perez-Aguilar, J. M.; Zhou, R. Mild Binding of Protein to C2N Monolayer Reveals Its Suitable Biocompatibility. *Small* **2017**, *13*, 1603685.
(119) Gu, Z.; Perez-Aguilar, J. M.; Meng, L.; Zhou, R. Partial Denaturation of Villin Headpiece upon Binding to a Carbon Nitride Polyaniline (C3N) Nanosheet. *J. Phys. Chem. B* **2020**, *124*, 7557−7563.
(120) Zhang, W.; Ye, C.; De Luna, P.; Zhou, R. Snatching the Ligand or Destroying the Structure: Disruption of WW Domain by Phosphorene. *J. Phys. Chem. C* **2017**, *121*, 1362−1370.
(121) Liu, R.; Zhai, H.; Meng, Y.; Zhu, M.; Wen, T.; Jin, N. Adsorption Behaviors of Typical Proteins on BP, GR, and C2N Surfaces. *J. Chem. Info. Model.* **2021**, *61*, 1300−1306.
(122) Craik, D. J.; Daly, N. L.; Bond, T.; Waine, C. Plant cyclotides: A unique family of cyclic and knotted proteins that defines the cyclic cystine knot structural motif. *J. Mol. Biol.* **1999**, *294*, 1327−1336.
(123) Craik, D. J. Seamless Proteins Tie Up Their Loose Ends. *Science* **2006**, *311*, 1563−1564.
(124) Colgrave, M. L.; Craik, D. J. Thermal, Chemical, and Enzymatic Stability of the Cyclotide Kalata B1: The Importance of the Cyclic Cystine Knot. *Biochem.* **2004**, *43*, 5965−5975.
(125) Simonsen, S. M.; Sando, L.; Ireland, D. C.; Colgrave, M. L.; Bharathi, R.; Göransson, U.; Craik, D. J. A Continent of Plant Defense Peptide Diversity: Cyclotides in Australian Hybanthus (Violaceae). *Plant Cell* **2005**, *17*, 3176−3189.
(126) Gracy, J.; Le-Nguyen, D.; Gelly, J.-C.; Kaas, Q.; Heitz, A.; Chiche, L. KNOTTIN: the knottin or inhibitor cystine knot scaffold in 2007. *Nucleic Acids Res.* **2007**, *36*, D314−D319.
(127) Pinto, M. A.-O.; Najas, J. Z. G.; Magalhães, L. G.; Bobey, A. F.; Mendonça, J. N.; Lopes, N. A.-O.; Leme, F. M.; Teixeira, S. P.; Trovó, M.; Andricopulo, A. D.; Koehbach, J.; Gruber, C. W.; Cilli, E. A.-O.; Bolzani, V. A.-O. Inhibition of Breast Cancer Cell Migration by Cyclotides Isolated from Pombalia calceolaria. *J. Nat. Prod.* **2018**, *81*, 1203−1208.
(128) Jennings, C.; West, J.; Waine, C.; Craik, D.; Anderson, M. Biosynthesis and insecticidal properties of plant cyclotides: The cyclic knotted proteins from Oldenlandia affinis. *Proc. Natl. Acad. Sci. U. S. A.* **2001**, *98*, 10614−10619.
(129) Ireland, D. C.; Wang, C. K. L.; Wilson, J. A.; Gustafson, K. R.; Craik, D. J. Cyclotides as natural anti-HIV agents. *Biopolymers* **2008**, *90*, 51−60.
(130) Pränting, M.; Lööv, C.; Burman, R.; Göransson, U.; Andersson, D. I. The cyclotide cycloviolacin O2 from Viola odorata has potent bactericidal activity against Gram-negative bacteria. *J. Antimicrob. Chemother.* **2010**, *65*, 1964−1971.
(131) Akhavan, O.; Ghaderi, E. Toxicity of Graphene and Graphene Oxide Nanowalls Against Bacteria. *ACS Nano* **2010**, *4*, 5731−5736.
(132) Ghosh, A.; Mukhopadhyay, T. K.; Datta, A. Two dimensional materials are non-nanotoxic and biocompatible towards cyclotides: evidence from classical molecular dynamics simulations. *Nanoscale* **2022**, *15*, 321−336.
(133) Keskin, O.; Gursoy, A.; Ma, B.; Nussinov, R. Principles of Protein-Protein Interactions: What are the Preferred Ways For Proteins To Interact? *Chem. Rev.* **2008**, *108*, 1225−1244.
(134) Ryan, D. P.; Matthews, J. M. Protein-protein interactions in human disease. *Curr. Opin. Struct. Biol.* **2005**, *15*, 441−446.
(135) Feng, M.; Kang, H.; Yang, Z.; Luan, B.; Zhou, R. Potential disruption of protein-protein interactions by graphene oxide. *J. Chem. Phys.* **2016**, *144*, 225102.
(136) Luan, B.; Huynh, T.; Zhou, R. Potential Interference of Protein-Protein Interactions by Graphyne. *J. Phys. Chem. B* **2016**, *120*, 2124−2131.
(137) Mukhopadhyay, T. K.; Ghosh, A.; Datta, A. Molecular Dynamics Simulations Reveal Orientation-Dependent Nanotoxicity of Black Phosphorene toward Dimeric Proteins. *ACS Appl. Nano Mater.* **2021**, *4*, 3095−3107.
(138) Mukhopadhyay, T. K.; Datta, A. Disentangling the liquid phase exfoliation of two-dimensional materials: an "in silico" perspective. *Phys. Chem. Chem. Phys.* **2020**, *22*, 22157−22179.
(139) Tu, Y.; Lv, M.; Xiu, P.; Huynh, T.; Zhang, M.; Castelli, M.; Liu, Z.; Huang, Q.; Fan, C.; Fang, H.; Zhou, R. Destructive extraction of phospholipids from Escherichia coli membranes by graphene nanosheets. *Nat. Nanotechnol.* **2013**, *8*, 594−601.
(140) Jimenez-Cruz, C. A.; Kang, S.-g.; Zhou, R. Large scale molecular simulations of nanotoxicity. *Wiley Interdiscip. Rev.: Syst. Biol. Med.* **2014**, *6*, 329−343.
(141) Zhou, R.; Gao, H. Cytotoxicity of graphene: Recent advances and future perspective. *WIREs Nanomed. Nanobiotechnol.* **2014**, *6*, 452−474.
(142) Mukhopadhyay, T. K.; Datta, A. Deciphering the Role of Solvents in the Liquid Phase Exfoliation of Hexagonal Boron Nitride: A Molecular Dynamics Simulation Study. *J. Phys. Chem. C* **2017**, *121*, 811−822.
(143) Yu, W.; He, X.; Vanommeslaeghe, K.; MacKerell, A. D., Jr Extension of the CHARMM general force field to sulfonyl-containing compounds and its utility in biomolecular simulations. *J. Comput. Chem.* **2012**, *33*, 2451−2468.
(144) Wang, J.; Wolf, R. M.; Caldwell, J. W.; Kollman, P. A.; Case, D. A. Development and testing of a general amber force field. *J. Comput. Chem.* **2004**, *25*, 1157−1174.

https://doi.org/10.1021/acsphyschemau.3c00053
ACS Phys. Chem Au 2024, 4, 97−121